
1 **This manuscript is a preprint** and has been submitted for publication in **Basin Research**.
2 It has been revised after peer review but **not yet accepted for publication**. Subsequent
3 versions of this manuscript may differ due to additional peer review or the editorial process.
4 If accepted for publication, the final version will be available through the “Peer-reviewed
5 publication DOI” link on EarthArxiv.
6 We hope you find this paper interesting and would welcome your feedback on it. Kindly
7 contact Folarin Kolawole (folarin.kol@gmail.com) with your feedback.
8

9 **Rift Transfer Zones and the Stages of Rift Linkage in Active Segmented**
10 **Continental Rift Systems**

11 Folarin Kolawole^{1*}, Max C. Firkins¹, Thuwaiba S. Al Wahaibi¹, Estella A. Atekwana², Michael
12 J. Soreghan¹

13

14 ¹School of Geosciences, University of Oklahoma, 100 East Boyd Street, RM 710, Norman, OK 73019

15 ²Department of Earth Sciences, University of Delaware, 101 Penny Hall, Newark, DE 19718

16 *Now at BP

17 *Corresponding Author: Folarin Kolawole (folarin.kol@gmail.com)*

18

19

20 **Abstract**

21 Although much is known about the interaction of faulting and sedimentation within the
22 basins of active segmented continental rift systems, little is known about these processes
23 within the transfer zones of varying geometries that separate the young interacting
24 segments. We address this problem in the humid, magma-poor juvenile western branch of
25 the East African Rift System (WB-EARS). First, we present a broader classification of rift
26 transfer zone geometries that accommodate both the plan-view geometries and border fault
27 polarity patterns of the interacting rift segments. Within the framework of the transfer zone
28 geometries, we explore the large-scale cross-over relief profiles, and the relationships with
29 the spatiotemporal development of rift-linking faults (breaching faults) and axial stream
30 patterns. Our results show that: 1.) distinct long-wavelength 2-D cross-over topographic
31 relief shapes, directionality of axial stream flow (sediment routing patterns), and breaching
32 fault patterns characterize rift transfer zones at the various stages of the linkage of
33 interacting rift basins, 2.) these stages include unbreached, partially-breached, recently-
34 breached, and breached transfer zones, 3.) deforming transfer zones exhibit different styles
35 of directionality of breaching, including a unidirectional (distinct propagator and receiver

36 segments) and bi-directional propagation (both segments act as propagators and receivers)
37 which may also modulate the cross-over relief shape, 4.) transfer zone breaching is
38 facilitated by rift-flank deformation, and/or rift tip propagation structures in the form of rift
39 splaying, border fault rotation, and fault cluster networks, 5.) the lateral propagation of
40 breaching faults at the rift tips and flanks may be modulated by the extension direction and
41 inherited basement structures. Our findings offer a broader insight into the geometries and
42 structural evolution of rift transfer zones, and provide first-order predictions of large-scale
43 sedimentation patterns of humid early-stage continental rift environments. Our models
44 provide testable hypotheses for linking rift architecture and patterns of early-stage
45 sedimentation applicable to ancient rift basins.

46

47 *Keywords: Continental rifting; Rift linkage; Transfer zones; Sedimentation; Normal faults.*

48 **1. Introduction**

49 Continental extension proceeds, first by the nucleation of discrete, isolated rift basin
50 segments which subsequently propagate laterally towards one another and link-up to form
51 continuous chains of rift basins (Figure 1, e.g., Nelson, et al., 1992; Corti, 2012; Zwaan et al.,
52 2016). The cross-over region of mechanical interaction between the propagating rift
53 segments leading to linkage is known as the rift transfer zone (Nelson, et al., 1992; Lambiase
54 and Bosworth, 1995; Heilman et al., 2019), which is larger in scale and distinguishable from
55 the relay zones that separate interacting normal fault segments (e.g., Morley et al., 1990;
56 Gawthorpe and Leeder, 2000).

57 The initial localization and structure of rift transfer zones are determined by a variety of
58 factors which include the inherited crustal mechanical anisotropies, variation in strain rate,
59 extension direction, magmatic focusing, border fault and rift geometries etc. (e.g., Bosworth,
60 1985; Morey et al., 1990; Acocella et al., 1999; Aanyu and Koehn, 2011; Corti, 2012; Heron et
61 al., 2019; Corti et al., 2019). However, rift segment interaction across deforming transfer
62 zones occurs in both the early (stretching) and later (necking and hyper-extension) stages
63 of continental rift development (e.g., Aanyu and Koehn, 2011; Pagli et al., 2018; Heilman et
64 al., 2019; La Rosa et al., 2019; Corti et al., 2019; Collanega et al., 2020). At continental break-
65 up, major transfer zones separating the offset segments of a rifted margin may influence the
66 location of subsequent oceanic transform fault development (e.g., Cochran and Martinez,
67 1988; Behn and Lin, 2000).

68 Rift transfer zones of active segmented continental rifts are areas of relatively elevated
69 basement which serve as viable source areas for sediment production and supply into the

70 active rift basins which constitute domains of crustal subsidence (Lambiase and Bosworth,
71 1995). In addition, rift transfer zones may accommodate intense tectonic stresses,
72 seismicity, and magmatism associated with tectonic interactions between active rift
73 segments that are in spatial proximity (Heilman et al., 2019; Corti et al., 2019).

74 Although climate and sea/lake level change play important roles in sedimentation along
75 continental rifts, the tectonic deformations impose first-order controls on sedimentation
76 patterns and stratigraphic architecture (e.g., Tiercelin et al., 1992; Lambiase and Bosworth,
77 1995; Soreghan and Cohen, 1996; Soreghan et al., 1999; Hans Nelson et al., 1999; Gawthorpe
78 and Leeder, 2000; Jackson et al., 2005; Mack et al., 2006). Within a given climatic condition,
79 active tectonics impose significant controls on the localization of uplifted zones where
80 erosion and sediment production occur, as well as on the localization of subsidence which
81 serve as depocenters for sediment accumulation (e.g., Hovius, 1998; Gawthorpe and Leeder,
82 2000; Barnes et al., 2011). Within these settings, the routing of sediments from the uplifted
83 areas into the depocenters are determined by the interplay between tectonic deformation
84 (e.g., spatiotemporal fault interactions), climate, dominant agents of sediment weathering
85 and transport, and base level change (e.g., Allen, 2008).

86 In evolving continental rift settings, the breaching and burial of cross-over basement-highs
87 between interacting rift basins (rift transfer zones) constitute the dominant signatures of rift
88 linkage and transformation of closed rifts into open rift basins (Gawthorpe and Leeder,
89 2000). However, there is limited understanding of how the morphology of rift transfer zones
90 evolve with the progression of tectonic and breaching fault interactions between the flanking
91 rift segment pairs. Also, there is a need to better understand how this evolution influences

92 the patterns of sediment routing into the basins, the linkage of the depositional systems, and
93 burial of the pre-existing basement-high of paleo-transfer zones.

94 The first-order characteristic of a rift transfer zone is its geometry (Nelson et al., 1992).
95 Therefore, the systematic assessment of the spatiotemporal evolution of a rift transfer zone
96 requires a consideration of the transfer zone geometry. However, the existing geometrical
97 classifications (Morley et al., 1990; Nelson et al., 1992) are limited, and do not encompass
98 the variety of transfer zone geometrical patterns that are observable along several
99 continental rift systems.

100 In this study, first, we re-assess transfer zone geometries and present a broader classification
101 that provides a better framework for assessing structure and evolutionary stages of rift
102 transfer zones. Within the framework of these transfer zone geometries, we investigate the
103 cross-over regions separating the active rift segments along the juvenile, humid, magma-
104 poor western branch of the East African Rift System (WB-EARS; Figure 2). Further, we
105 investigate the first order influence of fault breaching and basin-ward denudation on the
106 progressive deformation and burial of non-magmatic transfer zones, and the possible cross-
107 over topographic relief geometries associated with each sequential stage of the transfer zone
108 evolution.

109

110 ***1.1. Geologic Setting: The Western Branch of the East African Rift System (WB-EARS)***

111 The western branch of the Cenozoic East African Rift System (WB-EARS; Figure 2) is defined
112 by a N-S-trending arcuate-shaped system of elongate rift basin segments separated by
113 basement transfer zones, extending along the Proterozoic mobile belts separating Archean

114 cratons to the east and the west (e.g., Daly et al., 1989; Corti et al., 2007). This rift system
115 branch includes reactivated rift segments that had experienced the earlier phases of
116 Mesozoic extension recorded in east Africa. However, the Cenozoic and Mesozoic rifting
117 events were preceded by the Proterozoic continental accretion of the pre-rift basement. This
118 Precambrian basement of eastern Africa is composed of Proterozoic orogenic belts that wrap
119 around Archean cratonic blocks (Figure 2; Daly et al., 1989; Fritz et al., 2013). The rift system
120 propagates along and across the orogenic belts that flank the Tanzanian Craton to the west,
121 which include the Madi-Igisi, Ruwenzori, Ubendian, Kibaran, Irumide, Mozambique, and
122 Zambezi Belts (Figure 2). These mobile belts are dominated by gneisses with granulite and
123 amphibolite facies metamorphic rocks associated with terranes separated by steeply-
124 dipping shear zones and suture zones (Daly et al., 1989).

125 In the Phanerozoic, eastern Africa experienced at least three phases of continental extension.
126 These phases include the Permo-Jurassic 'Karoo' rifting, Cretaceous rifting, and the currently
127 ongoing Cenozoic phase of rifting (Delvaux, 1989). Some of the currently active segments
128 witnessed the Karoo phase of rifting and were reactivated during the subsequent rifting
129 episodes (e.g., Rukwa, North Malawi, Shire, Luano, and Luangwa Rifts in Figure 2). The
130 Cenozoic rift segments that make up the WB-EARS define a juvenile rift system (<25 Ma;
131 Roberts et al., 2012) extending from the Rhino Rift at its northernmost tip (where the rift
132 system terminates against the NW-trending Precambrian Aswa Shear Zone), southwards
133 through the Malawi Rift, Luangwa, Kundelungu, Mweru, and Kariba Rifts (Figure 2). The
134 southern portions of the western branch (e.g., Luangwa, Kundelungu, Mweru, Mweru-
135 Wantipa, Upemba, and Kariba Rifts) are also referred to as the 'southwestern' segments of

136 the rift system (Daly et al., 2020). In this paper, for simplicity, we consider these
137 'southwestern' rift segments to be part of the WB-EARS.

138 The WB-EARS yet remains an enigma, as it is largely magma-poor and its segments have
139 accommodated multiphase crustal stretching since Mesozoic times (Delvaux, 1989; Specht
140 and Rosendahl, 1989; Morley et al., 1999; Simon et al., 2017; Muirhead et al., 2018; Wright
141 et al., 2020). The WB-EARS is currently characterized by a maximum crustal stretching rate
142 of 2.9 mm/yr which is lower in comparison to that of the largely magma-rich eastern branch
143 (up to 5.2 mm/yr) of the East African Rift System, (EB-EARS; Saria et al., 2014). A few
144 magmatic centers occur along the WB-EARS and primarily at the rift transfer zones (Rungwe
145 Volcanic Province (RVP), South Kivu Volcanic Province (SKVP), Toro-Ankole Volcanic
146 Province (TAVP), Virunga Volcanic Province (VVP) in Figure 2). However, most of the
147 transfer zones are generally non-magmatic, showing no evidence of surface volcanism. The
148 absence of surface volcanism in several of the WB-EARS transfer zones present a 'simpler'
149 setting (i.e., one less tectonic variable) to explore the first-order dynamics of early-rift
150 linkage that characterize the growth of continental rifts and break-up process.

151

152 **2. Data and Methods**

153 We consider individual rift zones of a single or coalesced segments as discrete tectonic
154 elements within a rift system, which interact spatially when in proximity to one another.
155 Since active rift basins are zones of crustal subsidence, and the intervening cross-over region
156 separating the rifts prior to linkage (rift transfer zones; Figure 1) are regions of relatively

157 elevated basement, the linkage of the interacting rifts will require progressive structural
158 deformation, tectonic subsidence and burial of the cross-over region.

159 For a satisfactory assessment of the temporal evolution of rift linkage in an active continental
160 rift system as the EARS, we first evaluate the existing classifications of rift transfer zones,
161 examine the East African Rift system and other continental rift systems to create a more
162 robust and useful classification scheme. This updated classification scheme will provide a
163 basis for the definition of the cross-over spatial extents for various transfer zone geometries
164 (pink polygons in Figure 3) within which the assessment of breaching structures and cross-
165 over topography can be carried out.

166 To assess the status of the rift linkage at the rift transfer zones, we investigate the large-scale
167 patterns of active faulting and cross-over relief profiles across the transfer zone. More
168 specifically, we evaluate the similarities and differences in the general patterns of the large-
169 scale cross-over topographic morphology of the non-magmatic rift transfer zones along the
170 WB-EARS (Figure 4a) to identify the prominent trends (e.g., Figures 4b-g). Furthermore, we
171 analyze four representative transfer zones that span the possible stages of rift linkage
172 (unbreached, partial breaching, recent breaching, and breached) and contrast the
173 interactions between the tectonic structures and drainage systems in each case. In addition,
174 since the linkage of interacting rifts commonly transforms initially closed rift basins into
175 open basins (Gawthorpe and Leeder, 2000), we extend our assessments to include the first-
176 order trends and geomorphic characteristics of the axial streams that have catchment areas
177 in the transfer zones, and/or axial streams that flow across the lengths of the transfer zones
178 where observable.

179

180 **2.1. *Cross-Over Topographic Relief Profiles and Axial Stream Morphology***

181 We created topographic profiles of the transfer zones from the grids of the Global Multi-
182 Resolution Topography (GMRT) data (Ryan et al., 2009). The terrestrial component of the
183 GMRT data (used in this study) has a spatial resolution of ~30 m. To assess the long-
184 wavelength cross-over topographic geometries of the transfer zones, we plot topographic
185 profiles extending between the interacting rift segment pairs, parallel to and orthogonal to
186 the transfer zones where appropriate. We present the long-wavelength 2-D cross-over
187 profiles by both the moving average of the 30 m resolution GRMT data, and a profile of
188 resampled GMRT grid (resampled to 4 km resolution). The selection of the localities of the
189 longitudinal topographic profiles are primarily based on the large-scale structure of the
190 examined transfer zones. If there exists a zone of fault-bounded valleys linking the
191 interacting rifts (observable on the hillshade topographic and fault maps), we extend the
192 profile through the zone such that each end of the profile is in the axis of one of the two
193 interacting rift basins. If there is no observable linking fault-bounded valley in the transfer
194 zone, we place the topographic relief profile at any arbitrary location across the transfer
195 zone but ensuring that the two ends of the profile are in the axes of the rift basins. Due to the
196 unique geometry of overlapping parallel transfer zones, we orient the topographic profiles
197 in an across-strike manner (orthogonal to the longitudinal trend of the transfer zone).

198 We emphasize here that in all the WB-EARS transfer zones examined in this study, there is
199 no significant large-scale variation in the erodibility of the pre-rift basement lithologies as
200 the areas are primarily dominated by amphibolite-grade gneisses and granulites. In certain

201 areas, the metamorphic basement rocks have been intruded by pre-EARS igneous ring
202 complexes which show more resistance to erosion relative to the gneisses (e.g., Southern
203 Malawi Rift; Nyalugwe et al., 2019a). However, the locations of these igneous intrusions are
204 known, and they are also easily identifiable in the topographic hillshade and aeromagnetic
205 maps. In addition, the intrusions define short-wavelength structures and do not influence
206 the long-wavelength geometries of the important longitudinal topographic relief profiles
207 examined in our study areas. In areas where our profiles intersect the intrusions (e.g., across-
208 rift topographic profiles in Southern Malawi Rift), the intrusions are mostly at the rift margin
209 (border fault domain) and not along the flow path of the axial stream.

210 To investigate the relationships between the transfer zone cross-over topographic relief
211 geometry and the large-scale sediment routing patterns into the interacting rift basins, we
212 plot the longitudinal profiles of rift axial streams (permanent streams) that have catchments
213 in the transfer zones using elevation data from the GRMT grid. Although both the axial
214 streams and their tributaries provide sediments from the deforming and eroding transfer
215 zone basement-high into the subsiding rift basins, we envision that the large-scale
216 directionality of axial stream flow will more likely be controlled by the slope at the flanks of
217 the transfer zones.

218 The surface textures of the GMRT hillshade digital elevation model (DEM) maps can help
219 delineate the locations of recent alluvial sediment accumulation and areas of crystalline
220 basement exposures (Drury, 2001). Areas characterized by smooth textures on the DEMs are
221 interpreted as depositional surfaces reflecting primarily sediment accumulation and
222 aggradation, with erosion or gullying possibly present, but at a spatial scale lower than the

223 DEM resolution. Areas characterized by rougher textures on the DEM are interpreted as
224 regions of crystalline basement exposures where erosion dominates and produces
225 topographic relief on spatial scales greater than the pixel spacing of the DEM. Thus, to
226 delineate and map areas of subsidence and alluvial sediment accumulation at the
227 propagating tips of the active rift segments, we combine DEM hillshade maps and published
228 surficial geology maps of the study areas (e.g., Choubert et al., 1988). Further, we identify the
229 dominant border fault of a rift segment as the rift-bounding fault that is in the direction of
230 the downward tilt of the basin. Where available, we determine the border fault segments
231 from published seismic reflection images constrained by well log correlation (e.g., Albertine-
232 Rhino Transfer Zone). However, in areas where such subsurface data are absent, we
233 determine the direction of basin tilt from the overall direction of slope of the hanging wall of
234 the basin surface (e.g., Mack et al., 2006).

235

236 *2.1.1. Stream Sinuosity and Channel Width*

237 In humid continental settings such as the WB-EARS, the linkage of rift basin segments will
238 involve a transformation of at least a part of the transfer zone cross-over basement-high
239 (having significant surface slope gradients at the flanks prior to linkage) into a continuous
240 valley floor with significantly lower surface slope gradient after linkage. Since surface slope
241 patterns fundamentally control important geomorphic stream elements such as sinuosity
242 (Lazarus and Constantine, 2013), we assess the patterns of sinuosity along the relevant axial
243 streams.

244 Our study involves areas of basement exposure and burial along the rift floor near the
245 interacting rift segment tips, therefore, we quantify the variation of the channel width along
246 the axial streams to examine some aspects of the influence of rift-floor basement exposure
247 and transfer zone faulting on the large-scale geomorphology of the axial streams within some
248 of the transfer zones (e.g., see South Malawi–Shire, and Albertine-Rhino Transfer Zones).
249 Since the South Tanganyika-Rukwa Transfer Zone is a parallel transfer zone we examine two
250 major streams (Kalambo and “R1” Rivers) that although are not ‘axial’ to the interacting rifts,
251 are equally relevant to the study as they both initially flow parallel to the transfer zone before
252 deflecting into the interacting basins.

253 We manually digitized the active axial streams analyzed in the representative transfer zones,
254 and manually measured the stream widths (perpendicular to the stream channel) at regular
255 intervals along the stream channels using ArcMap© and Google Earth© satellite images.
256 However, due to the difference in the complexity of channel geometry between the study
257 areas (i.e., intensity of channel meandering, presence or absence of braided or anastomosing
258 sections), we varied the intervals used. We obtained measurements at 2 km regular intervals
259 in the Tanganyika - Rukwa Rift Transfer Zones (Kavuu and Luegele Rivers; cumulative
260 stream length of 300 km), 4 km regular intervals in the South Malawi - Shire Rift Transfer
261 Zone (Shire River; total stream length of 200 km), and 1 km regular intervals in the Albertine
262 - Rhino Rift Transfer Zone (Albert Nile River; total stream length of 105 km). At the braided
263 or anastomosing stream segments, we measure the width of the widest active channel. We
264 estimate channel sinuosity of major segments of the axial streams using standard approach.
265 To further assess the axial stream morphology anomalies where relevant, we utilize color

266 composites of Landsat TM optical satellite images obtained from the USGS Earth Explorer
267 database.

268

269 **2.2. Mapping of Sub-aerial and Subsurface Tectonic Structures**

270 *2.2.1. Fault Mapping*

271 To assess the structural deformation in active continental rift transfer zones (i.e., involving
272 at least one active rift segment), there is need for a detailed mapping of both the surface and
273 buried faults, as well as the pre-rift basement fabrics which often influence the patterns of
274 brittle strain localization (e.g., Heilman et al., 2019). In active rift basins, sub-aerial mapping
275 of faults from topographic hillshade maps and in the field are inherently limited because they
276 typically only reveal the recent surface-breaking active fault segments, and are generally not
277 able to delineate the buried active fault segments, which may be accommodating significant
278 tectonic strain (e.g., Kolawole et al., 2018). However, commonly available geophysical
279 datasets such as high-resolution aeromagnetic data provide subsurface imaging of both
280 intra-sedimentary and basement-rooted normal faults (Grauch and Hudson, 2007; Kolawole
281 et al., 2018). Due to the deep-penetrating nature of potential field geophysical signals,
282 aeromagnetic data allows us to discriminate between non-penetrative surface features (such
283 as river and paleo-lake terraces) and mega-scale penetrative structures such as faults and
284 mega-fractures. Unlike the mega-scale penetrative brittle deformation, non-penetrative
285 geological features do not create discontinuity lineaments that offset or disrupt the lateral
286 continuity of basement fabrics at the resolution of the aeromagnetic datasets utilized in this
287 study.

288 In the representative transfer zones analyzed in this study, we utilize the GMRT hillshade
289 DEM and previously published fault maps to delineate the sub-aerial fault segments. For
290 subsurface fault mapping, we evaluate previously published subsurface fault maps and
291 update the maps with subsurface fault interpretations from our filtered high-resolution
292 aeromagnetic maps. For example, in the Tanganyika - Rukwa Rift Transfer Zones, we include
293 and update the previously published surface fault lineaments mapped from satellite
294 topographic hillshade maps and field observations (Delvaux et al., 2012; Muirhead et al.,
295 2018). In the Southern Malawi - Shire Rift Transfer Zone, we include and update previously
296 published surface fault lineaments mapped from satellite topographic hillshade maps and
297 field observations (Wedmore et al., 2020). Also, in the Albertine - Rhino Rift Transfer Zone,
298 we include and update the previously published fault lineaments, some of which were
299 mapped from topographic hillshade maps, seismic reflection datasets, and in the field (GTK
300 Consortium, 2012; Westerhof et al., 2014; Katumwehe et al., 2015; Simon et al., 2017).
301 Therefore, in each of the three representative transfer zones analyzed in this study, we
302 identify several subsurface fault segments that are absent in previous publications, and
303 present updated fault maps which enable a detailed structural evaluation of the transfer
304 zone deformation.

305

306 *2.2.2. Mapping of Pre-rift Basement Fabrics*

307 In addition to fault mapping, we utilize the filtered aeromagnetic maps to image and
308 delineate the sub-aerial and buried pre-rift basement fabrics within the representative rift
309 transfer zones in order to better understand the controls on the breach faulting. In the study

310 areas, the pre-rift basement is metamorphic, dominated by gneisses and granulites with
311 mappable foliation trends (Figure 2). In the Tanganyika – Rukwa Rift transfer zone, SW
312 Tanzania, we use an aeromagnetic grid of 250 m spatial resolution, collected between 1977-
313 1980 with flight height of 200 m and a flight line spacing of 1 km (Supplementary Figure S1).
314 The Tanzanian aeromagnetic data was provided by the South Africa Development Council
315 (SADC). In the Southern Malawi – Shire Rift transfer zone, we utilize a 62 m-resolution
316 aeromagnetic grid, acquired in 2013 at a flight height of 80 m and 250 m flight line spacing
317 (Supplementary Figure S2). The southern Malawi data was provided by the Geological
318 Survey of Malawi (also, freely obtainable from Interdisciplinary Earth Data Alliance, IEDA;
319 Nyalugwe et al., 2019b). In the Albertine - Rhino Rift transfer zone, we utilize and update
320 previously published basement fabric interpretations from aeromagnetic data
321 (Supplementary Figure S3; Katumwehe et al., 2015, 2016). Prior to structural interpretation,
322 the Southern Malawi and SW Tanzania aeromagnetic grids were first reduced to the
323 magnetic pole (RTP), and the NW Uganda aeromagnetic data reduced to the magnetic
324 equator (RTE) in order to correctly locate the anomalies over their sources (Arkani-
325 Hamed, 1988). After the RTP and RTE corrections, we apply derivative filters to the grids to
326 resolve the structural features following examples of Arkani-Hamed (1988), Ma et al. (2012),
327 and Kolawole et al. (2018).

328 For our structural analyses, we generate rose diagrams of the frequency-azimuth
329 distribution of the faults and basement fabrics. For multimodal distributions, we divide the
330 data into their modal sets using the frequency minima; and for both the unimodal and
331 multimodal plots, we calculate the circular vector mean and 95 % confidence interval for the

332 modal sets using the method of Mardia and Jupp (2009). All the frequency-azimuth plots are
333 area-weighted.

334

335 **3. Results**

336 ***3.1. Re-assessment of Rift Transfer Zone Geometries***

337 Based on our observations of relative geometries of rift segments along the East African Rift
338 System and other continental rift systems, and an evaluation of previously published rift
339 transfer zone classifications (Morley et al., 1990; Nelson et al., 1992), we present a new
340 classification of rift transfer zone geometries (Figure 3). The terminologies adopted in our
341 new classification are descriptive and refer to the large-scale geometries of the interacting
342 rift segments. Further, where relevant, we include an additional term that accommodates a
343 secondary geometrical or structural component e.g., border fault polarity, and transverse
344 strike/oblique-slip faulting at rift tips.

345 In this new classification, we distinguish between paired rift transfer zones (involving only
346 2 rift segments) and compound rift transfer zones (involving >2 rift segments). For paired
347 rifts, we account for tip-to-tip, overlapping, and underlapping rift patterns of parallel,
348 oblique, and orthogonal trends of interacting rift pairs (Figure 3). Also, for compound rift
349 transfer zones, we account for triple junction (i.e involving 3 rift segments) and quadruple
350 junction (i.e. involving 4 rift segments) geometries. Further, we show three possible sub-
351 categories of quadruple junction transfer zones. In each class of transfer zone geometry, we
352 illustrate the possible lateral extents of the cross-over region.

353 Based on our new classification scheme for paired rift segments, we define profile transects
354 across the inter-rift cross-over regions in order to assess the general patterns of the transfer
355 zone relief geometries. The following section present our observations of the general
356 patterns of the relief geometries.

357

358 **3.2. Cross-Over Topographic Relief Profiles of Non-Magmatic Rift Transfer Zones along**
359 **the Western Branch of the East African Rift System (WB-EARS)**

360 Long-wavelength cross-over topographic relief profiles across the non-magmatic transfer
361 zones of different transfer zone geometries in the WB-EARS (Figure 4a) exhibit a variety of
362 shapes that can be broadly grouped into four major categories (Type-1 to Type-4) and a sub-
363 category (Type-3-4). We refer to the major categories as Type-1 to Type-4 morphologies
364 (Figures 4b-f). The Type-1 morphology is characterized by high relief; a topographic-high
365 surface, flanked on both sides by generally steep slopes that transition into topographic-low
366 surfaces of the interacting rift segments (e.g., Figure 4b). Examples of the Type-1 morphology
367 include the South Tanganyika–Rukwa (STR-TZ; 8°S, 31.5°E), Kundelungu–Luapula (KL-TZ;
368 10.25°S, 27.75°E), and the Central Luangwa–Central Malawi (CLCM-TZ; 12°S, 33.5°E) Rift
369 transfer zones (see Figure 4a for the locations). The Type-2 morphology is characterized by
370 less pronounced relief, but still exhibiting a topographic high surface flanked by a steeper
371 slope on one side and a less steep slope on the other side of the high (e.g., Figure 4c). An
372 example of the Type-2 morphology include the North Tanganyika-Rukwa Rift transfer zone
373 (NTR-TZ; 6.25°S, 30.5°E).

374 The topographic profile with Type-3 morphology is characterized by an elevated upper
375 surface that extends from the axis of one of the interacting rift segments. This surface ramps
376 steeply down to a lower elevation surface in the adjacent segment (e.g., Figure 4d). Type-3
377 morphology examples include the Southern Malawi–Shire (SMS-TZ; 15.75°S, 34.75°E) and
378 the Zambezi-Kafue (ZK-TZ; 16°S, 28.5°E) Rift transfer zones. Finally, the Type-4 morphology
379 features a considerably flat topographic relief profile that extends between the axis of the
380 two interacting rift segments (Figure 4f). Examples of Type-4 morphology includes the

381 Albertine–Rhino (AR-TZ or BTZ; 2.7°N, 31.4°E), and the Shire-Urema (SU-TZ; 16.85°S,
382 35.35°E) Rift Transfer Zones.

383 However, we also observe another morphology type that has a form of Type-3 morphology,
384 but has more undulations on its ramp than the typical Type-3 morphology (Figure 4e). We
385 dub this the ‘Type-3-4’ morphology. Except for the Upemba-Kundelungu transfer zone (UK-
386 TZ; 9.15°S, 26.75°E), we commonly observe this morphology at the transfer zones where
387 active EARS segments overlap and overprint unreactivated Karoo rift basins. Examples
388 include the Ruhuhu–Malawi (RM-TZ; 10.75°S, 34.75°E), Maniamba–Malawi (MM-TZ; 12. 5°S,
389 34.8°E), and Luama–Tanganyika (LT-TZ; 5.9°S, 29.2°E) Rift transfer zones (Figure 4a). Along
390 the Type-3-4 relief profile, the unreactivated Karoo basin extends from the ramp into the
391 elevated part of the transfer zone topographic relief profile.

392 Below, we focus on representative Type-1 to Type-4 transfer zones along the WB-EARS and
393 present observations of the pre-rift basement fabrics, faulting patterns, and axial drainage
394 patterns and anomalies. We focus on the STR-TZ, NTR-TZ, SMS-TZ, and AR-TZ, due to the
395 presence of accessible datasets that are relevant to our investigation. Due to the change in
396 the transfer zone geometry along the Tanganyika - Rukwa Rift cross-over zone (caused by
397 along-strike change in the Tanganyika Rift trend), we separate the transfer zone into a
398 northern (NTR-TZ) and southern (STR-TZ) domain.

399

400 ***3.3. Representative Type-1 Morphology Transfer Zone: The South Tanganyika-*** 401 ***Rukwa Rift Transfer Zone (STR-TZ)***

402 The STR-TZ is an overlapping-parallel divergent transfer zone that is located between the
403 Rukwa rift and the NW-trending southernmost segment of the Tanganyika rift (Figure 5a).
404 The transfer zone cross-over region, known as the Ufipa Horst, is essentially the uplifted
405 basement horst between the Ufipa Fault footwall and the adjacent Tanganyika Rift (Figures
406 5a-c). This transfer zone has recorded significant seismic activity, ranging from $M_w < 3.7$ up
407 to $M_w 7.4$ (Figure 5a; Vittori et al, 1997).

408

409 *3.3.1. Pre-rift Basement Fabrics and Rift Faulting in the STR-TZ*

410 The metamorphic foliation (i.e., 'basement fabrics') of the STR-TZ basement revealed in the
411 filtered aeromagnetic grid (Figures 5b-c), show dominant NW-SE trends with $148^\circ \pm 4.3$ mean
412 orientation (Figure 5d). Likewise, mapped faults (Figure 5c) within the transfer zone show
413 the same prominent trend, with a mean of $147^\circ \pm 3.2$ (Figure 5e). On a larger-scale, we
414 observe that the trends of the South Tanganyika Rift and its east bounding faults, as well as
415 trends of the Rukwa Rift, its west bounding fault (Ufipa Fault), and the Kanda Fault (major
416 fault in the transfer zone; Figure 5f) are parallel to the dominant NW-SE trend of the
417 basement fabrics. In this transfer zone, we do not observe the presence of prominent cross-
418 faulting that directly links the Rukwa and South Tanganyika Rift basins.

419

420 *3.3.2. Axial Stream Morphology in the STR-TZ*

421 The axial streams within the transfer zone (e.g., Kalambo(KIR), Momba (MR), Mfuizi (MfR),
422 and R1 Rivers) generally flow parallel to the long-axis of the transfer zone and are confined

423 to narrow valleys that are bounded by steep fault scarps (Profile P1; Figures 5a and 5f).
424 Downstream, the streams change course and flow into the interacting rift segments of Lake
425 Tanganyika (in Tanganyika Rift) and Lake Rukwa (in the Rukwa Rift) (Figures 5a and 5g).
426 The longitudinal profiles of representative axial streams (Kalambo and R1, which flow in
427 opposite directions) show steepening of the profile with associated waterfalls (e.g. Kalambo
428 Waterfall) along both the eastern and western flanks of the transfer zone. Additionally, at the
429 flanks of the transfer zone, the streams commonly show a significant decrease in channel
430 width and sinuosity relative to the upstream sections that extend well into the transfer zone
431 (e.g., Kalambo River, Figure 5g).

432

433 ***3.4. Representative Type-2 Morphology Transfer Zone: The North Tanganyika-*** 434 ***Rukwa Rift Transfer Zone (NTR-TZ)***

435 The NTR-TZ has an overlapping-oblique divergent geometry, and is located between the
436 northwestern tip of the Rukwa rift and the central segment of the Tanganyika rift (Figures
437 5a and 6a-b). Similar to the STR-TZ, this northern transfer zone has recorded significant
438 seismic activity, including multiple $M_w > 5.0$ events (Figure 5a).

439

440 ***3.4.1. Pre-rift Basement Fabrics and Rift Faulting in the NTR-TZ***

441 The basement fabrics of the NTR-TZ show a dominant NW-SE trend observable on the
442 aeromagnetic map (Figure 6a) with a mean of $139^\circ \pm 5.2$ (Figure 6c). Also, the mapped faults
443 in the transfer zone (Figure 6b) show a prominent NW-trend with a mean of $137^\circ \pm 3.4$
444 (Figure 6d), parallel to the basement fabrics. The mean trends of both the basement fabrics

445 and faults in this transfer zone are slightly oblique to those of the South Tanganyika - Rukwa
446 transfer zone, suggesting an anticlockwise deflection in the trend of the structures. This
447 deflection is apparent in the fault map of the transfer zones (Figure 5a).

448 Overall, the faults within the NTR-TZ form a network that extends northwestwards from the
449 tip of the Rukwa Rift and links up with faults along the eastern boundary of the Tanganyika
450 Rift (Figure 6b). The transfer zone-orthogonal topographic profiles (Figures 6e-g) show that
451 at the NW tip of the Rukwa Rift, the basin is defined by a broad sediment-filled valley (smooth
452 DEM surface texture) bounded by a low-gradient ramp that transitions to low-relief rift
453 shoulders (Profile P2; Figure 6e). Further northwest, into the transfer zone (Profile P3;
454 Figure 6f), the basin morphology is characterized by multiple narrow sediment-filled
455 troughs (narrow zones of smooth DEM surface texture) bounded by steep fault scarps and
456 higher relief shoulders.

457 Proximal to the Tanganyika Rift (Profile P4; Figure 6g), the surface morphology of the
458 transfer zone is characterized by ubiquitous basement exposures with rare occurrence of
459 significant sediment accumulation (rougher DEM surface textures). Two moderate
460 magnitude ($M_w > 5.0$) earthquakes in the NTR-TZ show strike-slip kinematics with at least
461 one nodal plane trending parallel to the mean fault trend and mean basement fabric trend
462 (Figures 5a, 5d-e). However, near the Rukwa Rift tip, the events generally show oblique
463 normal faulting (Figure 5a).

464

465 *3.4.2. Axial Stream Morphology in the NTR-TZ*

466 The Type-2 topographic morphology of the NTR-TZ (Figure 6h) features a central
467 topographic-high flanked to the northwest (towards the Tanganyika Rift) by a steep
468 escarpment, and to the southeast by a gentle slope that extends into the axis of the Rukwa
469 Rift. Several humps and steps occur along the gentle slope and are collocated with the
470 prominent NE-SW trending ridges (Figure 6h) that were formed by paleo-shorelines of Lake
471 Rukwa (Figure 5a; Delvaux et al.,1998).

472 Within the transfer zone, the axial streams (Kavuu (KR) and Luegele (LR) Rivers) diverge
473 away from the central topographic-high (shared catchment region) and drain into the
474 interacting rift basins (Figure 6h). The Luegele River flows northwest over a distance of ~55
475 km and drains into the Tanganyika Rift. The Luegele River steepens at ~28-30 km along the
476 profile (Figure 6i) which is collocated with the steep escarpment that bounds the transfer
477 zone to the northwest. Within this steeper reach, the Luegele River is characterized by rapids
478 (Luegele Rapids). We observe that although the channel width shows an abrupt decrease
479 across the steep elevation gradient, the sinuosity index of the channel shows an increase on
480 the downslope segment of the river (Figure 6i). The Kavuu River flows southeastwards from
481 the transfer zone and drains into the Rukwa Rift (Figure 5a). Although the channel extends
482 over a longer distance (> 260 km) and transects a gently sloping topography (Figure 6i), the
483 sinuosity and width of the channel show systematic variations. Two prominent anomalies
484 are observable on the stream profile; these include an abrupt elevation step that is collocated
485 with the Ilyandi Ridge and a change to a steep gradient at the Maimba Ridge (Figure 6i).
486 Furthermore, we observe that the Kavuu River attains peak sinuosity index (~1.58) and
487 channel width just upstream of two of the ridges, the Ilyandi Ridge and Rungwa Ridge. Each
488 of these ridges is located just downstream of a prominent small lake (e.g., Lake Katavi) or

489 swamp (Figure 5a). However, overall, the sinuosity of the axial streams is higher than those
490 of the STR-TZ.

491

492 **3.5. Representative Type-3 Morphology Transfer Zone: The South Malawi-Shire Rift** 493 **Transfer Zone (SMS-TZ)**

494 The SMS-TZ encompasses the southernmost tip of the Malawi Rift, essentially the Zomba
495 Graben which is located between the Shire Horst and the Shire Rift (Figures 4a and 7a).
496 Based on the overall trend of the Malawi Rift relative to the Shire Rift, we describe this cross-
497 over region to be an overlapping-oblique divergent transfer zone.

498

499 **3.5.1. Pre-rift Basement Fabrics and Rift Faulting in the SMS-TZ**

500 To better understand the distribution of metamorphic basement fabrics and faulting in the
501 SMS-TZ (Figures 7b-c), we analyze the structures in the northern and southern parts of the
502 Zomba Graben separately. The North Zomba Graben is distal to the Shire Rift, and the South
503 Zomba Graben is proximal. The metamorphic fabrics of the North Zomba Graben are defined
504 by curvilinear magnetic fabrics (Figure 7b) trending NNE-SSW ($014^{\circ}\pm 4.1$) (Figure 7di),
505 parallel to the rift faults (Figure 7dii). In the South Zomba Graben, the metamorphic fabrics
506 show bimodal trends with NNE-SSW ($029^{\circ}\pm 3.9$) and NW-SE ($144^{\circ}\pm 4.2$) sets (Figure 7ei) in
507 which only the NNE set shows strong correspondence to a prominent fault set (Figure 7eii).
508 The faults in the South Zomba Graben show multimodal trends with NNE-SSW ($023^{\circ}\pm 4.6$),
509 NNW-SSE ($164^{\circ}\pm 5.7$), and ENE-WSW (079°) (Figure 7eii). The border faults of the South
510 Zomba Graben generally follow basement fabrics, and although most of the intra-basinal

511 faults and fractures crosscut the pre-rift fabrics, some segments locally follow the basement
512 fabrics (Figure 7c).

513 The border faults of the Zomba Graben exhibit synthetic geometry mostly prominent in the
514 south Zomba Graben. In the northern Zomba Graben, the intra-basinal faults dominantly
515 trend NNE-SSW, parallel to the trend of the graben (Figure 7dii). In the south Zomba Graben,
516 intra-basinal deformation is characterized by a cluster of faults/mega-fractures (breaching
517 faults) generally trending NNW, and extend northwestward from the footwall of the Thyolo
518 Fault, the border fault of the Shire Rift into the axis of the Zomba Graben (Figures 7a and 7c).
519 The Thyolo Fault itself extends northwestwards, and in the region of overlap with the Zomba
520 Graben, it rotates clockwise into a NNW-trend and continues as a mega-fracture through the
521 axis of the Zomba Graben to link up with the western border fault system (Lisungwe Fault
522 (LsF); Figures 7a and 7c).

523

524 *3.5.2. Basin Morphology and Axial Stream Morphology in the SMS-TZ*

525 Within the SMS-TZ (Figure 8a), the axial stream, the Shire River flows southward from Lake
526 Malombe (Malombe Graben, Figures 8a-b), through the Zomba Graben and continues into
527 the Shire Rift. The first-order trend of the Shire River is characterized by a systematic shift
528 in the along-rift axial location of the stream. In the north (Malombe Graben), the river is
529 located near the center of the rift (Figure 8c), whereas, in the North Zomba Graben, the river
530 is located near the eastern border fault (Chingale Step Fault) (Figure 8d). From this location,
531 the river deflects southwestwards such that its position is again at the rift axis within the

532 central segment of the Zomba Graben (Figure 8e), but further south, is located near the
533 western border fault of the graben (Lisungwe Fault, Figure 8f).

534 In addition, we observe that although the Malombe Graben is characterized by a graben
535 (Figure 8b) to asymmetric graben (Figure 8c) geometries, the Zomba Graben presents an
536 along-rift flip in the polarity of the basin morphology. In the North Zomba Graben the
537 direction of the tilt of the basin is eastward (green arrow in Figure 8d) but flips to a westward
538 tilt in the southern part of the rift (green arrow in Figures 8e-f). Essentially, the variations in
539 the along-rift location of the Shire River are consistent with the along-rift change in the
540 polarity of the basin and location of the dominant border fault.

541 We also observe that the morphology of the Shire River transitions from a relatively flat
542 elevation profile upstream within the Malombe Graben and North Zomba Graben (Upper
543 Shire River), through a steep profile in the South Zomba Graben (Middle Shire River), to a
544 flat topography in the Shire Rift (Lower Shire River; Figure 8g). Along the Upper Shire River,
545 the channel width mostly varies between 33 - 187 m with a sinuosity index of ~ 1.17 but
546 decreases significantly to 15 - 130 m channel width and 1.04 sinuosity index in the Middle
547 Shire River. Along the Lower Shire River, both the channel width and sinuosity index
548 increase to values much higher than those of the Upper Shire River (60 - 215 m channel
549 width and 1.28 sinuosity index; Figure 8g). Although the Upper Shire River is generally
550 sinuous and curvilinear in geometry (Figure 8a), there exists two prominent localized zones
551 of significantly high sinuosity patterns where the river exhibits anastomosing characteristics
552 (anastomosing sections in Figures 8a and 8h). Whereas, the Middle Shire River exhibits
553 major rectilinear and orthogonal geometries, some of which align with mapped fault and

554 mega-fracture lineaments (e.g., Figure 8i). The Lower Shire River is highly sinuous
555 throughout its length as it flows on the hanging wall of the Thyolo Fault (e.g., Figure 8j).

556

557 **3.6. Representative Type-4 Morphology Transfer Zone: The Albertine-Rhino Rift**
558 **Transfer Zone (AR-TZ, a.k.a. BTZ)**

559 The AR-TZ is defined by the NNW-trending Butiaba Transfer Zone (BTZ) which is located
560 between the NE-trending Albertine Rift to the south and the NE-trending Rhino Rift to the
561 north (Figures 4a and 9a). This transfer zone, also known as Pakwach Basin (Zwaan et al.,
562 2016), is an underlapping-parallel divergent transfer zone.

563

564 **3.6.1. Pre-rift Basement Fabrics and Rift Faulting in the BTZ**

565 Within the BTZ, the basement fabrics show a prominent ENE-WSW trend ($066^{\circ}\pm 9.3$), with
566 secondary NE-SW ($033^{\circ}\pm 9.3$) and E-W ($094^{\circ}\pm 8.0$) trends (Figure 9b). However, we observe
567 that the BTZ faults dominantly strike NNE-SSW ($027^{\circ}\pm 5.4^{\circ}$), oblique to the trend of the
568 transfer zone (Figure 9c). Faulting in the BTZ is characterized by two main fault networks,
569 both of which extend from two of the three prominent splay faults at the northern tip of the
570 Bunia border fault of the Albertine Rift (“Splay-1, -2, & -3” in Figure 9a). The westernmost
571 strand (Splay-1) connects to a network of short tightly clustered en-echelon faults, bounding
572 the BTZ to the west and southwest which extends northwards to link up with the western
573 border fault of the Rhino Rift (Figure 9a). The central splay (Splay-2) connects to a network
574 of longer faults, the most prominent of which is the Ragem Fault, which extend across the

575 BTZ into the footwall of the eastern border fault of the Rhino Rift. The easternmost splay
576 (Splay-3) also extends across the BTZ and appear to link up with the Splay-2 fault network.
577 Overall, fault segments of Splay-3 appear to bound the BTZ to the east and northeast (Figures
578 9a and 9e). In the Rhino Rift, the border fault systems terminate at the NW-trending
579 Precambrian Aswa Shear Zone (Figure 9a).

580

581 *3.6.2. Basin Morphology and Axial Drainage Patterns in the BTZ*

582 The Albert Nile and Victoria Nile Rivers represent the major axial drainage systems of the
583 Albertine Rift. However, the Albert Nile River is the primary axial drainage system that
584 drains both the Albertine and Rhino Rifts, and the BTZ between them (Figure 9a). Although
585 the first-order trend of the Albert Nile River is generally sub-parallel to the trend of the
586 transfer zone, we observe that the along-rift locations of the river are collocated with the
587 dominant border fault locations. The river flows northwards from the Lake Albert which is
588 bounded by the border faults of the Albertine Graben (Figures 9a and 9d). In the BTZ, the
589 basin surface morphology shows a consistent northeastward-tilt, and the Albert Nile channel
590 flows along the northeastern boundary of the transfer zone (Figure 9a, 9e, and 9f). Within
591 the Rhino Rift, the basin morphology is characterized by a southeastward-tilt (towards the
592 Rhino Fault), and the Albert Nile flows along the hanging wall of the Rhino Fault (Figures 9a
593 and 9g). Further north, closer to the rift termination at the Aswa Shear Zone, the river
594 deflects towards the northwestern border fault (Figure 9a).

595 Overall, the entire longitudinal elevation profile of the Albert Nile River describes a relatively
596 'flat' topography with very wide segments (77 – 1,800 m width) characterized by large

597 meanders and highly anastomosed morphology (Figure 10a-10e). We observe two broad
598 partitions on the Albert Nile River morphology profile which consists of a northern and
599 southern partition, separated by the Ragem Fault (Figures 10a and 10b). The southern
600 partition consists of a single wide channel within a relatively narrower valley, featuring
601 sparse anastomosing sections with wide stream branches (Figures 10a, 10b, 10c, 10d). The
602 northern partition is characterized by a wider river valley of continuously anastomosing
603 river segments with narrow stream branches and a high density of lakes (Figures 10a, 10b,
604 10e). The morphology of the northern partition of the river extends along most of the entire
605 length of the Rhino Rift. On the hanging wall of the Ragem Fault, the river valley defines a
606 roughly fault-parallel (NNE) trend, whereas, in the footwall of the fault, the river valley
607 rotates into a fault-perpendicular (NNW) trend (Figure 10b). Additionally, we observe an
608 abrupt narrowing of the river channel across the Ragem Fault such that a wide lake (1.35
609 km-wide) ponds within the hanging wall of the fault and drains into a narrow (~300 m-wide)
610 channel on the footwall of the fault (Figures 10b and 10d).

611

612 **4. Discussion**

613 **4.1. *A New and Broader Classification of Rift Transfer Zones***

614 The existing geometrical classification of rift transfer zones (Morley et al., 1990; Nelson et
615 al., 1992) are useful, but are significantly lacking in that they do not encompass the variety
616 of transfer zone geometrical patterns that can be observed in modern continental rift
617 systems. Also, the existing schemes are overly simplistic, and either only considered the
618 plan-view rift geometries (Nelson et al., 1992) or border fault dip polarity for only parallel

619 rift pairs (Morley et al., 1990). The classifications do not allow the analyses of complexities
620 arising from multiphase extension with varying extension directions, and generally ignore
621 the possible temporal evolution from one rift transfer zone geometry into another. Here, we
622 establish a unifying broader classification scheme that accommodates the plan-view
623 geometries, polarity patterns (dip direction) of interacting border faults, and temporal
624 transformation of the rift transfer zone geometries (Figure 3).

625 Our new classification scheme features both paired (involving only 2 rift segments) and
626 compound (involving >2 rift segments) transfer zones. Along the WB-EARS (Figure 4a), a few
627 examples of the geometries shown in the new scheme include: Tip-to-tip collinear (Rukwa-
628 North Malawi), Overlapping parallel divergent (Upemba-Kundelungu, Kundelungu–Luapula,
629 South Tanganyika – Rukwa Transfer Zones), Overlapping orthogonal divergent (Tanganyika-
630 Mweru Wantipa Transfer Zone), Overlapping oblique divergent (Luama–Tanganyika
631 Transfer Zone), Complex quadruple junction (Rukwa-Luangwa-North Malawi–Usangu
632 Transfer Zone). In other continental rift systems, examples include Overlapping oblique
633 (South Viking–Witch Ground Transfer Zone, North Sea Rift), Overlapping oblique divergent
634 (Wetterau–Leine Transfer Zone, European Cenozoic Rift System), Overlapping parallel
635 divergent (Utsira High, North Sea Rift; Limagne–Bresse Transfer Zone, European Cenozoic
636 Rift System), Overlapping oblique convergent (Española–San Luis Transfer Zone, Rio
637 Grande Rift), Overlapping parallel convergent (Albuquerque-Española Transfer Zone, Rio
638 Grande Rift), Overlapping orthogonal divergent (Lower Rhine–Upper Rhine Transfer Zone,
639 European Cenozoic Rift System), and Underlapping parallel divergent (Upper Rhine-Bresse
640 Transfer Zone, European Cenozoic Rift System).

641 For each category of transfer zone, we show the lateral extents of the cross-over region
642 across which the breaching faults would develop and propagate. Also, we indicate the
643 possible variations of the breaching distances across the cross-over regions, indicating the
644 areas within the cross-over region where relatively shorter distances of fault propagation
645 could facilitate breaching. We note that the configuration of some of the rift transfer zone
646 geometries suggest a possible temporal transformation from one geometry to another. For
647 example, in paired rift transfer zones, depending on the stress field orientation and inherited
648 basement structures, with continued extension, unfaulted underlapping transfer zones can
649 evolve into an overlapping geometry or faulted underlapping geometry. Also, stress rotation
650 between rifting episodes in multiphase rifts can lead to the transformation of a paired rift
651 transfer zone geometry into a compound transfer zone geometry (e.g., Turkana Depression,
652 Fairhead, 1988; Emishaw et al., 2019; Morley, 2020).

653 Most numerical and analog models of rift linkage have been limited in scope because they
654 only investigated parallel rift transfer zones (underlapping and overlapping parallel transfer
655 zones, e.g., Acocella et al., 1999; Corti, 2004; Zwaan et al., 2016; Zwaan & Schreurs, 2017). An
656 example of this limitation is the assumption that the Rukwa Rift represents a strike-slip
657 transfer zone between the Tanganyika Rift and Malawi Rift (e.g., Zwaan & Schreurs, 2017)
658 even though faults of the Rukwa Rift largely exhibit normal faulting kinematics (e.g., Morley
659 et al., 1999; Morley, 2010; Lavayssière et al., 2019). Although models successfully reproduce
660 the temporal transformation from a type of parallel transfer zone into another, there remains
661 the need to consider the wider variety of rift transfer zone geometries as shown our updated
662 classification scheme. Overall, we clarify that the geometries shown in our new scheme are

663 most representative of early-stage continental extension, as the complexity of structural
664 deformation intensifies with the progression of continental extension towards break-up.

665 In the following sections, within the framework of our transfer zone geometrical
666 classification for paired rift segments, we analyze and discuss the detailed characteristics of
667 four representative transfer zones along the Western Branch of the East African Rift System
668 (WB-EARS, Figure 4a). Based on the structural and morphotectonic characteristics of each
669 of the cross-over regions examined, we infer the likely stage of evolution of the transfer zone,
670 the patterns of breach faulting and the basement controls.

671

672 **4.2. Rift Interactions at the South Tanganyika-Rukwa Rift Transfer Zone (STR-TZ)**

673 The STR-TZ is an excellent example of Overlapping parallel divergent transfer zone (Figures
674 2 and 5a). The prominent topographic-high and steep flank morphology of the Ufipa Horst
675 (Type-1 morphology, Figure 4b), and the presence of waterfalls and rapids on the flanks
676 (Figures 4b, 5f-g) suggest that the Ufipa Horst is actively uplifting along both of its flanks.
677 This uplift is likely associated with the flexural footwall uplift of the Ufipa Fault (bounds the
678 Rukwa Rift to the southwest) and that of faults bounding the south Tanganyika Rift to the
679 northeast. The clear correlation between the trends of basement metamorphic fabrics and
680 faults within the horst block (Figures 5d and 5e) indicate a clear control of the pre-rift
681 basement fabrics on strain accommodation within the transfer zone. In addition, the near-
682 orthogonal orientation of the extension direction relative to the dominant basement fabric
683 trends (Figures 5a and 5d-e) implies that the deformation of the transfer zone could be
684 accommodated by normal fault exploitation of the pre-rift basement fabrics. However, the

685 complexity of kinematics of the deformation in the STR-TZ is demonstrated by the
686 prominence of Cenozoic oblique-normal and strike-slip faulting, with minor reverse faulting,
687 possibly associated by local SHmin rotation (Delvaux et al., 2012; Lavayssière et al., 2019).

688 The mapped faults are parallel to the long axis of the Ufipa Horst with no major graben
689 system connecting the Rukwa and Tanganyika Rifts (Figures 5b-c), and the crust which
690 appears to have been intruded by magma, is relatively thicker than those of the flanking rifts
691 (Hodgson et al., 2017; Lavayssière et al., 2019). The deformation of this transfer zone is
692 relatively less intense in comparison to the overlapping parallel NLNM-TZ where the North
693 Rukuru-Mwesia Rift and Henga Rift (NRR and HR in Figure 4a) represent a transfer zone-
694 parallel deformation of the cross-over region (Ring, 1995). Likewise, it is less intense in
695 comparison to the deformation of the N-S-trending Limagne-Bresse Transfer Zone by the
696 NNW-trending Roanne-Forez graben system in the European Cenozoic Rift System (Dèzes et
697 al., 2004). Whereas, another overlapping parallel transfer zone, the UK-TZ (Figure 4a) is
698 breached by a major transverse structure (here in referred to as the “Lufira Fault, LF” in
699 Figure 4a) with well-developed sediment-filled valley (Choubert et al., 1988) and a through-
700 going axial stream (Lufira River) which physically link the Upemba and Kundelungu Rift
701 basins. Thus, we infer that the presence of lower-crustal magma intrusions and the
702 development of the Kanda and Kalambo-Mwimbi Fault Systems possibly indicates the
703 initiation of rifting within the STR-TZ (Figures 5c and 5f). Therefore, our preferred
704 interpretation is that the STR-TZ is a partially breached transfer zone. However, we also
705 suggest that the breaching of overlapping parallel transfer zones can occur by the
706 development of transverse faulting (UK-TZ) and/or pervasive development of transfer zone-
707 parallel subsidiary rift basins (STR-TZ, NLNM-TZ, and Roanne-Forez graben). The UK-TZ is

708 a breached transfer zone, the structure of which the STR-TZ could evolve into with
709 progressive extension (and/or future rotation of the regional SHmin orientation).

710

711 **4.3. Rift Interactions at the North Tanganyika-Rukwa Rift Transfer Zone (NTR-TZ)**

712 The NTR-TZ represents an overlapping oblique divergent transfer zone. The shape of the
713 topographic relief profile extending from North Tanganyika Rift to Rukwa Rift (Figure 6h)
714 shows that, in contrast to the steeper NW flank of the transfer zone (Tanganyika Rift), the SE
715 flank (towards the Rukwa Rift) is characterized by a longer stretch of gently-sloping
716 topography. Along this long stretch of gentle topography, the first-order axial stream trends
717 are parallel to the fault and basement fabric trends (indicating large-scale control of tectonic
718 fabrics).

719 Multiple narrow troughs develop at the NW tip of the Rukwa Rift passing into the transfer
720 zone (Figures 6b and 6f). These narrow troughs are bounded by actively propagating fault
721 networks that extend northwest across the transfer zone towards the eastern margin of the
722 northern Tanganyika Rift. Thus, we interpret that the development of the Type-2
723 topographic relief shape across the NTR-TZ is influenced by a progressive northwestward
724 propagation of the NW tip of the Rukwa Rift towards the northern Tanganyika Rift (Figures
725 6b and 6e-g). Further, the clustering of earthquakes at the NW Rukwa Rift tip and within the
726 SE part of the transfer zone suggests that active crustal deformation is partitioned to the
727 southeastern half of the NTR-TZ, as well as an active northwest-ward propagation of the
728 Rukwa Rift tip (Figure 5a; see clustering of relocated earthquakes in Lavayssière et al., 2019).
729 Several of the mapped faults extend from the tip of the Rukwa Rift into the interior of the

730 transfer zone. We suggest that the relative steepness of the northern flank of NTR-TZ 2-D
731 cross-over relief profile (Figure 6h) is representative of an absence of pronounced
732 southeastward propagation of rifting from the Tanganyika flank of the NTR-TZ. The NTR-TZ
733 faults represent transfer zone breaching faults and are accommodating a mix of strike-slip
734 and oblique-normal slip kinematics (Figures 5a, 6b, and 6f; Lavayssière et al., 2019).

735 We interpret that the NTR-TZ is a partially breached transfer zone, in which the Rukwa Rift
736 is the active propagator, and the north Tanganyika Rift is the 'receiving' segment. Further,
737 the active propagation of the Rukwa Rift tip is accompanied by splaying of the rift tip into
738 multiple troughs. The moderate magnitude strike-slip faulting ($M_w > 5$) in the interior of the
739 NTR-TZ (Figure 5a) is compatible with the WNW-ESE regional extension direction and
740 counterclockwise rotation of fault and basement fabric trends from the STR-TZ to NTR-TZ
741 (Figures 5d-e, 6c-d). However, the presence of oblique normal faulting near the Rukwa Rift
742 tip (Figure 5a; Lavayssière et al 2019) possibly indicates local stress rotations (Morley,
743 2010). Local rotations of the SHmin orientation into fault-orthogonal trends have also been
744 highlighted in the northern Malawi Rift (Kolawole et al., 2018) and southern Malawi
745 (Williams et al., 2019). Overall, the alignment of fault trends and basement fabric trends
746 (Figures 5d-e) suggest that at gross-scale, the transfer zone breaching is associated with an
747 exploitation of the inherited basement fabrics.

748 We note that in the region of STR-TZ to NTR-TZ transition, some fault lineaments extend
749 from the Chisi Fault (northernmost segment of Ufipa Fault System) to the Tanganyika Rift
750 (Figure 5a). This transition region shows more seismic activity than the interior and
751 southern regions of the STR-TZ (Lavayssière et al-2019). However, these faults do not form

752 a well-developed continuous valley (i.e., insignificant fault displacement). Although the
753 Nkamba River (NR in Figure 5a) extends across the faults and up to a watershed divide in
754 the footwall of the Chisi Fault, the river only served as a fluvial link between Lakes Rukwa
755 and Tanganyika during transient phases of overflowing of Lake Rukwa (Cohen et al., 2013).
756 Thus, with the progressive strain accommodation in the STR-TZ to NTR-TZ transition zone,
757 a breaching graben and permanent fluvial linkage valley could evolve.

758 Finally, our observations show that the 1st-order trends, flow directions, and longitudinal
759 relief gradients of the axial streams indicate a dominant direction of transfer zone breaching.
760 The Kavuu River (axial stream) originates at the termination zone of one of the splay troughs
761 where the distal segment of the stream shows the channel width of the axial stream is
762 generally smaller and less sinuous (Figure 6i). Whereas further SW in the Rukwa Rift, the
763 river exhibits higher sinuosity and channel width, and geomorphic features associated with
764 lake-level fluctuations (Lake Rukwa paleo-shorelines; Figures 5a and 6i; Delvaux et al., 1998)
765 which are controlled by coupled tectonics and paleoclimatic conditions (Delvaux et al.,
766 2011).

767

768 **4.4. Rift Interactions at the South Malawi-Shire Rift Transfer Zone (SMS-TZ)**

769 The border faults of the Zomba Graben are the southern continuation of the Malawi Rift
770 border fault systems (Figure 7a). Thus, being the southernmost segment of the rift, the
771 Zomba Graben represents the transfer zone between the Malawi Rift and the Shire Rift. In
772 the northern part of the Zomba Graben (distal to the Shire Rift), the intra-basinal and border
773 faults are mostly parallel or sub-parallel and trend NNE, except for a few NE and ENE steps

774 along the border faults (Figure 7a and 7dii). The alignment of the fault trends with the
775 orientation of the pre-rift basement fabrics indicates a control of basement fabrics on fault
776 geometries (Figure 7c, 7di and 7dii). Whereas basement fabrics and rift faulting in the South
777 Zomba Graben appear to be relatively more complex, and the intra-basinal faults define an
778 NNW-trending fault/mega-fracture cluster which is oblique to the NE-trend of the Zomba
779 Graben and border faults (Figures 7a, 7c). This intra-basinal fault cluster extends NNW from
780 the footwall of the Thyolo Fault (Shire Rift active border fault) into the axis of the South
781 Zomba Graben, exhibiting soft- and hard-linkage patterns with the Zomba Graben border
782 faults (Lisungwe, Zomba, and Chingale Step Faults) and the North Zomba intra-basinal faults
783 (Mlungusi and Mtsimukwe Faults).

784 The clockwise rotation of the northwestern tip of the Thyolo border fault from a NW trend
785 to NNW trend is guided by a pre-existing basement shear zone (Figure 7c and inset; Morel,
786 1958), but is also well-oriented to be reactivated in the current ENE extension direction.
787 Also, we note that although the breaching fault cluster in South Zomba Graben generally
788 trend NNW, some of the segments locally crosscut- while others follow the basement fabrics
789 (Figure 7c). Although the current extension direction (Figure 7a) is favorable for the
790 reactivation of the NNE- and NW-trending border faults of the Zomba Graben and Shire Rift
791 (Williams et al., 2019), the NNW-trend of the breaching fault cluster segments is even more
792 optimally-oriented for reactivation in this regional stress field. Therefore, we infer that the
793 breach faulting of the SMS-TZ exhibits a partial control of pre-rift basement structures, but a
794 stronger control of the tectonic extension direction. In summary, we suggest that there exists
795 an appreciable structural linkage between the border faults of the Shire Rift and Zomba

796 Graben, and that the deformation is compatible with the current stress field and is partially
797 associated with local exploitation of pre-rift basement fabrics.

798 The consistency between the along-rift alternation of basin polarity (basin tilt direction, e.g.,
799 Mack et al., 2006) and the along-rift changes in the location of the main axial stream (Shire
800 River) indicates the first-order control of rift structure on axial drainage pattern in the
801 Zomba Graben (Figures 8b-f). The alignment of a segment of the Shire River with a collocated
802 buried fault and dike (white arrows in Figures 7a and 7c) may also indicate a secondary
803 structural control on the stream geometry. However, more importantly, the morphology of
804 the transfer zone relief profile (south-facing ramp/step; Type-3 morphology) indicates a
805 unidirectional southward flow pattern across the transfer zone (Figure 8g), along-trend of
806 which the pre-rift basement is broadly exposed at the rift floor and is flanked to the east and
807 west by the graben border faults (Figures 8a and 8i). This zone of exposed basement on the
808 rift floor is collocated with the Middle Shire River where the axial stream longitudinal profile
809 becomes steeper and is dominated by waterfalls, rapids, narrowed channel, and fracture-
810 controlled stream segments (Figures 8g and 8i). The waterfalls and rapids mostly cluster in
811 the northern part of the area of the rift-floor basement exposure where the Shire River
812 follows the limb of a plunging fold structure (see Figures 7b-c, and 8a and 8g) and there is
813 no observable large igneous dikes or basement lithologic contacts (i.e., contacts separating
814 hard and soft rocks) cross-cutting the river channel at the location of the waterfalls.
815 Therefore, these observations all together, indicate that although the SMS-TZ is breached,
816 the breaching is most likely a recent event. The waterfalls likely occur at knick points that
817 develop as the stream attempts to adjust to a new longitudinal drainage profile (supported
818 by observations in Bloomfield, 1965; Dunlavy, 2017).

819 The southern Malawi Rift evolved through the episodic southward propagation of the
820 Malawi Rift (Scholz et al., 2020), subsequently leading to its tectonic interaction with the
821 eastern sub-basin (Lower Shire sub-basin) of the Shire Rift Zone. The North Zomba Graben
822 is dominated by paleo-lake sedimentary deposits (Matope Beds and associated lacustrine
823 clays) of Neogene age or younger which directly overlie the Precambrian basement
824 unconformity surface, and are overlain by the alluvial sediments of the Shire River
825 (Bloomfield and Garson, 1965; Thomas et al 2009; Lyons et al 2015; Dunlaya, 2017;
826 Wedmore et al 2020). This shallow paleo-lake (or swamp) developed within a structural-low
827 land area (fault-bounded?) surrounded by basement uplifts from which sediments were
828 sourced into the lake (Dunlaya, 2017). In essence, the paleo-lake was restricted to the south
829 by an elevated basement area, which separated the lake from the Shire Rift. Based on paleo-
830 environmental reconstruction and consideration of likely provenance of the paleo-lake
831 sediments, it was concluded that linkage of the Upper and Lower Shire River segments (i.e.,
832 linkage of the Zomba Graben and Shire Rift depositional environments) is a 'recent' feature
833 (Dunlaya, 2017). The observations of a previously restricted depocenter in the North Zomba
834 Graben are consistent with our analyses, emphasizing that the present-day location of the
835 South Zomba Graben (Middle Shire River segment) must have been an elevated basement
836 region in pre-Quaternary times. Thus, the progressive brittle deformation, erosion, and
837 subsidence of the uplifted cross-over region (in the Quaternary) facilitated the continuous
838 south-directed flow of the axial stream (Shire River) from the Lakes Malawi and Malombe,
839 through the south Zomba area, into the Lower Shire sub-basin of the Shire Rift.

840 We suggest that the breaching of the SMS-TZ is facilitated by both the NW-NNW propagation
841 of the Thyolo Fault (active border fault of the Shire Rift Zone) and the concurrent southward

842 propagation of the Zomba Graben border faults, largely guided by the current extension
843 direction. An early-rift localization of significant intra-basinal strain in the Zomba Graben
844 has been highlighted but is inferred to be possibly controlled by a deeper lower-crustal
845 mechanical heterogeneity along the rift axis (Wedmore et al., 2020). However, the basement
846 fabrics (which represent exhumed lower-crustal structures) do not show the presence of a
847 discrete pre-rift terrain boundary along the rift axis (Figure 7b); rather the fabrics show a
848 north-plunging fold structure. Although, the large fold structure extends across the entire
849 rift width, the large-scale aeromagnetic character of the basement fabrics changes across the
850 western border fault (Lisungwe Fault) and the more significantly across the eastern border
851 fault system (Chingale Step and Zomba Faults) (Figures 7b-c; also see Nyalugwe et al., 2019a,
852 2020). Thus, the prominent mechanical weaknesses of the exhumed basement occur
853 primarily along the border fault zones and not the intrabasinal domain of the Zomba Graben.
854 Therefore, we suggest that this early-stage intra-basinal strain localization in the Zomba
855 Graben can also be explained by the recent breaching of the rift transfer zone and migration
856 of strain into the axis of the Zomba Graben through the breaching fault/mega-fracture
857 clusters.

858

859 ***4.5. Rift Interactions at the Albertine–Rhino Rift Transfer Zone (AR-TZ, a.k.a. Butiaba*** 860 ***Transfer Zone, BTZ)***

861 The Butiaba Transfer Zone (BTZ) represents the transfer zone between the Albertine and
862 Rhino Rifts. The BTZ is bounded by a tight cluster of short en-echelon faults to the southwest
863 and relatively longer fault segments to the southeast and northeast (Figure 9a). Although the

864 basement fabrics show a multimodal trend (Figure 9b), a secondary NNE-trending set is
865 parallel to the dominant fault trend (Figure 9c). We observe that two major breaching fault
866 systems extend from the NW border fault of the Albertine Rift (Bunia Fault), across the BTZ,
867 and soft-link or hard-link with the border faults of the Rhino Rift. These two systems include
868 the tight cluster of short en-echelon faults that appear to link up with the western Luku
869 border fault of the Rhino Rift, and a system of fault splay consisting of three 'large' fault
870 strands that extend towards the southern tip and footwall of the Rhino border fault of the
871 Rhino Rift (Figure 9a). These BTZ breaching fault systems are sub-orthogonal to the crustal
872 stretching direction, are locally parallel to a pre-rift fabric trend, and oblique to the trend of
873 the BTZ (Figure 9a and 9c). Also, the extension direction is moderately oblique to the rift
874 trends, consistent with analog modelling results (Zwaan et al., 2016). Overall, these
875 geometrical relationships suggest that the brittle deformation of the BTZ exploited the
876 basement fabrics in an oblique rifting tectonic setting.

877 The axial stream longitudinal profile is very flat in this region, and the river itself is
878 characterized by generally large channel widths (Figure 10a), suggesting a low energy
879 equilibrated axial stream. The morphology of this axial stream profile relative to those of the
880 other representative transfer zones analyzed in this study is quite unique and indicative of
881 the evolutionary stage of the transfer zone. Seismic reflection imaging of a part of the BTZ
882 that is proximal to the Albertine Rift reveals ~2 km sedimentary fill (Simon et al., 2017),
883 indicating a relatively significant basin subsidence in the transfer zone. This magnitude of
884 subsidence in the BTZ is important, considering that prior to the structural deformation and
885 subsidence across a transfer zone, the cross-over region must have been an elevated
886 basement area (see analog models in Zwaan et al., 2016). These observations lead us to infer

887 that the Albertine – Rhino Rift Transfer Zone is indeed a breached transfer zone, and that
888 any paleo-intervening basement-high is faulted (footwall blocks of Ragem Fault and Bunia
889 Fault Splay-3) and buried, and the axial stream now simply flows across its own floodplain.
890 However, it is much likely that as continental extension progresses, the present structure of
891 the transfer zone will continue to evolve. Also, if the Ragem Fault continues to propagate
892 further northward into the footwall of the Rhino Rift, prominent overlapping geometries
893 may develop between the Rhino and Albertine Rifts. The change in the trend of the axial
894 stream river valley (fault-parallel trend in the SE to fault-perpendicular trend in the NW) and
895 the partitioning of axial stream morphology anomalies by the Ragem Fault (Figures 10a-e)
896 demonstrate the continued structural control on the large-scale axial stream morphology in
897 a breached transfer zone.

898

899 **4.6. The Stages of Rift Linkage in Non-Magmatic Continental Rift Transfer Zones**

900 *4.6.1. Distinguishing Topographic Morphologies and Sediment Routing Patterns*

901 Based on the structure of the representative transfer zones, the associated axial stream, and
902 long-wavelength topographic relief geometries, we present four possible sequential stages
903 of rift linkage in active juvenile continental rift systems (left panel of Figure 11). These stages
904 include 1) unbreached, 2) partially breached, 3) recently breached, and 4) breached rift
905 transfer zones. Further, based on the observed directionality of axial stream flow and
906 location of rift-related sediment deposition, we present an idealized stratigraphic evolution
907 of the sedimentary stratigraphy of the interacting rift basins (middle and right panels of
908 Figure 11).

909 Prior to rift linkage, the intervening transfer zone is essentially a relatively elevated
910 basement region with steep flanks relative to the axes of the interacting rift basins
911 (unbreached, Stage 1; Figure 11a). At this stage, the axial streams of the two rifts with
912 sources in the cross-over region are not linked, such that a bi-directional pattern of sediment
913 dispersal (2-D perspective along cross-over profile) from the transfer zone into the rift
914 basins will likely dominate. However, with the progressive growth of the propagating rift
915 tips, the breaching faults propagate further into the transfer zone cross-over region, and with
916 continued erosion, allows for the migration of subsidence into the transfer zone. Thus, with
917 continued extension, the transfer zone evolves into a narrowed cross-over basement-high
918 (asymmetric or symmetric) or faulted horst block (if fault-bounded e.g., overlapping parallel
919 transfer zones), a stage which we describe as a “partially breached transfer zone” (Stage 2;
920 Figure 11b). The NTR-TZ, STR-TZ, and the Luano-Kafue Transfer Zone (LK-TZ) exhibit
921 characteristics that demonstrate this stage of rift linkage. We suggest that the cross-over
922 topographic relief geometries of a Stage 2 transfer zone will likely be strongly dependent on
923 the directionality of propagation of rift linkage and spatial variation of basement erodibility.

924 With continued propagation of the breaching faults, the rift bounding faults of the interacting
925 rift segments establish connection (through soft and/or hard linkage) and one or more well-
926 developed rift valleys develop across the transfer zone. Where the linkage creates a
927 continuous rift valley floor connecting the interacting rift basins, axial stream reversal occurs
928 and a common axial stream may develop, exhibiting unidirectional flow between the
929 interacting rifts. At this initial stage of successful establishment of rift linkage, we refer to the
930 transfer zone as a “recently breached transfer zone” (Stage 3; Figure 11c). The SMS-TZ and
931 ZK-TZ (Figure 4a) clearly exhibit characteristics that fit this stage of rift linkage. We clarify

932 that 'recent' as used in the context of "recently breached transfer zones" is qualitative,
933 relevant to modern active continental rift environments.

934 The transition from Stage 2 to Stage 3 facilitates the evolution of the interacting rifts from
935 hydrologically closed basins to open ones as their depositional systems become linked (e.g.,
936 Gawthorpe and Leeder, 2000). Also, we highlight the possible prominence of capturing
937 and/or reversals of antecedent axial streams flowing into the interacting rift basins as the
938 transfer zone cross-over region transitions from Stage 2 to Stage 3. However, it should be
939 noted that apart from strain rates on breaching faults, how quickly a Stage 2 transfer zone
940 (partially breached) transitions into Stage 3 can be significantly determined by basement
941 structure and lithological heterogeneity, which often impact the rates of fluvial erodibility
942 and drainage divide mobility patterns within the uplifted cross-over region (e.g., Annandale,
943 1995; Zondervan et al., 2020). Also, the fluvial erodibility and drainage divide mobility
944 within the deforming transfer zone prior to linkage, and the rate of sediment filling in the
945 interacting basins at the Stage 3 will potentially influence the transition from one stage to
946 another.

947 Finally, with the continued coalescence of the linked breaching and border fault systems of
948 the interacting rifts, the transfer zone cross-over topography becomes progressively worn
949 down by the axial drainage system and its transverse streams as unidirectional flow of the
950 axial stream dominates. Also, the axial stream longitudinal profile attains the form of a low
951 energy equilibrated axial drainage system. We refer to this stage as "breached transfer zone"
952 (Figure 11d). Thus, in humid continental rift settings where sedimentation rates are keeping
953 up with strain rates on faults, the breaching of transfer zones and structural linkage of

954 interacting rift segments are important for persistent drainage network connectivity and
955 sediment transport between the interacting rift segments.

956 We note the common occurrence of the Type-3-4 morphology at the transfer zones
957 separating active EARS and unreactivated Karoo rifts (e.g., Figure 4e). The exception is the
958 UK-TZ where the interacting rifts although are EARS segments, contain Karoo sedimentary
959 rocks (Choubert et al., 1988). We interpret that this morphology indicates a transfer zone
960 that is breached, in which the breaching may or may not be 'recent'. However, more
961 importantly, the morphology represents a breached transfer zone in which the axial stream
962 has not yet equilibrated. Where a Type-3-4 cross-over morphology connects a failed Karoo
963 rift and an overlapping active EARS segment, the Karoo basin may be located in the elevated
964 part of the profile due to the flexural uplift of the flanks of the active EARS basin. Therefore,
965 as a result of the elevated location of the failed rift, its sedimentary or volcanic rift-fill will
966 undergo erosion and incision by streams as the deposits are reworked into the linked
967 actively subsiding rift basin. The case of Type-3-4 cross-over morphology connecting two
968 active rift segments may indicate an imbalance of sediment supply rate relative to strain rate
969 between the two linked active rift segments creating an overfilled versus an underfilled
970 segment.

971 Although the models presented in Figure 11 demonstrate our observations in WB-EARS, and
972 idealizations in aspects for which we do not have field observations, they assume 1) humid
973 continental setting, 2) orthogonal extension, 3) the erodibility of the pre-rift basement is
974 relatively uniform, 4) sediment supply in the interacting basins keeps up with strain rates
975 on faults, and 5) no significant influence of dynamic topography within the deforming

976 transfer zones. In addition, we clarify that these models are relevant for regions of active
977 early-stage continental rifting. Our study suggests that for a given directionality of breaching,
978 paired rift transfer zones that are not fault-bounded or are fault-bounded on only one flank
979 will show distinct long-wavelength 2-D topographic relief shapes that indicate the stage of
980 transfer zone breaching (Figure 11). Therefore, 2-D topographic profiles across an
981 unbreached transfer zone should exhibit a Type-1 morphology, and a breached transfer zone
982 should exhibit profiles shapes of Type-3, Type-3-4, or Type-4. Based on our observations of
983 deformation patterns in various overlapping parallel transfer zones, it appears that this
984 category of transfer zone is unique in that the attainment of breaching may either involve
985 the development of cross-faulting that extends across the intervening horst block and/or the
986 development of subsidiary rift basins within the horst block. However, in the case of a
987 development of subsidiary rift basins (e.g., NLNM-TZ, Figure 4a; Limagne–Bresse Transfer
988 Zone), breaching of the transfer zone must involve the structural connectivity of the
989 subsidiary basins with at least one of the interacting rift segments and unidirectional flow of
990 the axial stream between both.

991 Since the linkage of interacting rift segments is manifested in the physical linkage of their
992 intra-basinal and/or border fault segments, we infer that the post-linkage phase of
993 interacting rifts may show a record of accelerated strain and subsidence across the breached
994 transfer zone (Figures 11d and 12; Gawthorpe and Leeder, 2000). The linkage and
995 coalescence of propagating fault segments often lead to increased strain accommodation and
996 basin subsidence rates along the newly linked faults (e.g., Gupta et al., 1998; Gawthorpe and
997 Leeder, 2000; Taylor et al., 2004; Cowie et al., 2005). In the Whakatane Graben, New Zealand,
998 for example, the post-linkage displacement rate of the major normal faults increased by up

999 to threefold (Taylor et al., 2004). The unavailability of high-resolution data on fault
1000 displacement rates at the representative WB-EARS transfer zones analyzed in this study
1001 makes it currently difficult to test this hypothesis. Therefore, there is a need to better
1002 understand the significance of the temporal variations of breaching fault displacement rates
1003 for the evolution of rift transfer zones. Overall, we emphasize that post-linkage, coalesced
1004 rift basins may preserve a buried record of paleo-transfer zones that indicate the location of
1005 an initial phase of separated rift segments and progressive breaching and rift linkage (Figure
1006 12).

1007

1008 *4.6.2. Directional Propagation of Transfer Zone Breaching and Rift Linkage*

1009 The separation distance between active rift segments determines if and how they will
1010 interact spatially (e.g., Tentler and Acocella, 2010; Zwaan et al., 2016). Thus, with continued
1011 tectonic extension, an isolated rift segment may continue to propagate laterally until its
1012 breaching distance (distance from another rift segment) is small enough to permit
1013 interaction and development of breaching faults in the transfer zone cross-over area. In this
1014 study, our observations at the representative non-magmatic rift transfer zones reveal two
1015 distinct styles of rift propagation associated with transfer zone breaching (Figure 12). In one
1016 case, we observe that only one of two interacting rift segments acts as the propagating
1017 segment (i.e., the ‘propagator’) such that the other ‘non-propagating’ segment represents the
1018 ‘receiver’, demonstrating a unidirectional style of transfer zone breaching and rift linkage.
1019 For example, in the NTR-TZ (Figure 6), the Rukwa Rift represents the propagator, and the
1020 Tanganyika Rift represents the receiver. Also, in another case, we find evidence that suggests

1021 that both interacting segments propagated towards one another, indicating a bi-directional
1022 style of transfer zone breaching (e.g., SMS-TZ; Figures 7-8).

1023 We clarify here, that in areas of multiphase rifting where younger rift basins may propagate
1024 across older failed rift basins, the younger active rift represents a propagator, and the
1025 ‘inactive’ (or partially active) older rift segment represents a receiver. In the representative
1026 transfer zones analyzed in this study, we find that within the larger-scale framework of a
1027 transfer zone geometry, the lateral propagation of breaching faults may be modulated by the
1028 extension direction and inherited basement structures. Further, based on the pattern of
1029 seismicity clustering in the NTR-TZ (Figure 5a), we suggest that in transfer zones with
1030 adequate seismic station coverage, the spatial distribution of seismicity clustering
1031 (representing a partitioning active crustal deformation) provide insight into the
1032 directionality of transfer zone breaching.

1033

1034 *4.6.3. Rift-Tip and Rift-Flank Interactions*

1035 Models of interaction between parallel rift pairs (i.e., parallel transfer zones) have
1036 demonstrated how the obliquity or orthogonality of extension direction can influence the
1037 patterns of rift-tip interactions and geometry of breaching faults in homogeneous media and
1038 in the presence of a connecting pre-existing fault (e.g., Acocella et al., 1999; Aanyu and Koehn,
1039 2011; Zwaan et al., 2016; Zwaan and Schreurs, 2017). Model results and the natural
1040 examples examined in our study show that the breaching of rift transfer zones is facilitated
1041 by complex patterns of structural deformation that link the interacting rift basins.

1042 On a large-scale, we find that transfer zone breaching is commonly facilitated by propagating
1043 rift-tip (e.g., in tip-to-tip collinear, and underlapping transfer zones) and/or rift-flank
1044 deformation (e.g., in overlapping oblique and parallel divergent transfer zones). In our
1045 current study of the WB-EARS, we observe that propagating rift-tips may be characterized
1046 by 1) rift splay creating a pattern of smaller and narrower graben and/or half-grabens (e.g.,
1047 rift bifurcations, rift trifurcations etc.), 2) rotation of the propagating border fault tip, and/or
1048 3) network of fault clusters, that extend into deforming transfer zones. An example of rift-
1049 flank deformation is the breaching of the UK-TZ, NLNM-TZ, and SMS-TZ (Figures 4a and 12a).
1050 Whereas examples of rift splay include splay troughs at the NW Rukwa Rift tip, bifurcation
1051 of the SE Rukwa Rift tip, trifurcation (or greater) of the NW Luama Rift tip, bifurcation of the
1052 northern Edward Rift tip, splay faulting at the northern Albertine Rift tip (Figures 4a and
1053 13a). An example of border fault rotation is the clockwise rotation of the NW tip of the Thyolo
1054 border fault in the SMS-TZ. Also, examples of transfer zone breaching by fault cluster
1055 networks include the Butiaba Transfer Zone (AR-TZ), and SMS-TZ (Figures 7a and 9a).

1056 We suggest that rift splay and border fault rotation are analogous to the geometries of fault
1057 networks that have been observed at the laterally propagating fault tips (e.g., Kim et al.,
1058 2004; Perrin et al., 2016; Phillips et al., 2019). Although rift splay was previously presented
1059 as a class of rift transfer zones (Nelson et al., 1992), we argue here that rift-tip splay and
1060 border fault rotation represent genetic characteristics of long-term lateral propagation of
1061 continental rift-tips. Thus, such structures, although not the transfer zone itself, could
1062 suggest that a propagating rift segment is approaching a termination or an interaction zone
1063 with another segment. This is also consistent with observations in numerical models where
1064 border fault rotation at transfer zones indicates lateral propagation and interaction of rift

1065 segments and can be controlled by the extension direction (Zwaan et al.,2016). Thus, the
1066 preservation of the rift-tip structures highlighted in this study within the syn-rift fill of
1067 composite rift basins (i.e., coalesced segmented rifts) may provide insight into previous rift-
1068 tip locations and zones of interaction with another rift segment prior to linkage. An example
1069 of a buried bifurcation zone is the Northern Malawi Rift at the Likoma-Lipichilli Horst
1070 (Specht and Rosendahl, 1989), which is collocated with the inferred earlier termination of
1071 the Malawi Rift (Scholz et al; 2020). Also, an example of buried border fault rotation zone is
1072 in the central Tanganyika Rift where the rift is segmented across the Kavala Island Ridge - a
1073 transfer zone which is now breached and is currently undergoing burial as seen in seismic
1074 interpretations (Wright et al., 2020). Interestingly, the Rwenzori Transfer Zone between the
1075 Edward and Albertine Rifts show both well-developed bifurcation and border fault rotation
1076 (Koehn et al., 2008).

1077 At zones of rift slays, it appears that at least one of the splay branches (splay trough) may
1078 eventually 'fail' while one or more branches continue to localize most of the tectonic strain
1079 and facilitate a successful linkage with the interacting rift segment. For example, the Songwe
1080 Trough of the SE Rukwa Rift bifurcation has localized greater strain and breaching of the
1081 Rukwa-North Malawi Transfer Zone (Mbozi block) than the Musangano Trough (Heilman et
1082 al., 2019). Additionally, the Malombe Graben of the Southern Malawi Rift bifurcation is a
1083 better-developed bifurcation branch than the Bilila-Mtakataka Trough as evidenced by the
1084 continuation of the rift valley floor, axial stream linkage (Shire River), and localization of a
1085 major lake (Lake Malombe) along the Malombe Graben (Figures 7a, 8a and 8c; see also
1086 Dunlaya, 2017).

1087 Overall, our analyses show that although rift transfer zones may differ in both their
1088 geometries and evolutionary stages, there exist distinct long-wavelength 2-D cross-over
1089 relief profile geometries that are unique to each of the evolutionary stages within a given
1090 erodibility structure, breaching propagation directionality, strain rate, and sediment-supply
1091 rate across the transfer zone. We envision that our observations in this study provide
1092 predictive models for the geometry and temporal evolution of paleo- rift transfer zones
1093 preserved in the stratigraphic record of mature continental rifts and passive margin basins.
1094 However, we acknowledge that further refinement of these models should be undertaken
1095 with additional studies of both ancient and modern systems.

1096

1097 ***4.7 Implications for Early-Stage Continental Rift Growth in East Africa***

1098 Along the eastern Africa rift zones analyzed in this study, based on the long wavelength
1099 cross-over relief morphology, fluvial isolation/linkage of interacting rifts, and the general
1100 breaching fault patterns at the transfer zones, we find that at least 60 % of the rift transfer
1101 zones exhibit characteristics of breaching (Figures 13a and 13b). We characterize all
1102 magmatic transfer zones as “breached” because of the lithospheric-scale deformation
1103 associated with magmatism. Several of the Mesozoic rift segments (pre-EARS) show
1104 characteristics of breaching across the transfer zones (fault connectivity and
1105 proximity/overlapping of rift-fill e.g., Kariba-Zambezi, Ruhuhu–Malawi, Maniamba-Malawi,
1106 Luangwa-Zambezi, and Shire-Zambezi Rift Transfer Zones; Figure 13a). The development
1107 and lateral propagation of the Cenozoic rift segments have facilitated their linkage with the
1108 Mesozoic rift segments (Delvaux, 1989). Overall, we note that the northern regions of the

1109 WB-EARS and the southern regions of the EB-EARS appear to be dominated by breached
1110 transfer zones, whereas the rift segments further south show more of partially breached,
1111 recently breached, and unbreached transfer zones (Figure 13a). The apparent southward
1112 and southwest-ward increase in the occurrence of unbreached, partially breached, and
1113 recently breached transfer zones reflects the proposition of an active southwest-ward
1114 propagation of the East African Rift System (Daly et al., 2020).

1115 Cenozoic continental extension in the EARS initiated ~40 Ma (Boone et al., 2019), and its
1116 Western Branch (WB-EARS) evolved ~25 Ma (Roberts et al., 2012), such that by the Middle
1117 Miocene to Pliocene, most of the rift segments had been established (Simon et al., 2017;
1118 Scholz et al., 2020). However, the predominance of breached transfer zones along these
1119 juvenile branches of the East African Rift System (Figure 12a), suggest that the early-stage
1120 establishment of the EARS segments is associated with considerable transfer zone breaching
1121 and rift linkage. Although the EARS is actively growing, the early-development of most of its
1122 segments is consistent with observations of early-stage rapid establishment of segments in
1123 the East Greenland rift system (i.e., within the first 20 % of rift life; Rotevatn et al., 2018).
1124 Therefore, we propose that the continued southwest-ward growth of the EARS (Daly et al.,
1125 2020; Ngalamo et al., 2020) will likely record continued lateral propagation of the rift tips,
1126 linkage across the rift transfer zones, intensified deformation and burial of the recently
1127 breached and paleo-transfer zones.

1128

1129

1130

1131 **4.8 Outstanding Questions**

1132 It was suggested that small scale tensile fractures are possible analogs of actively
1133 propagating continental rift segments (Nelson et al., 1992). Heilman et al. (2019) further
1134 speculated that the laterally propagating rift tips are zones of stress concentration with a
1135 distinct ‘process zone’, and that rift transfer zones are areas of overlap between the process
1136 zones of rift segments that are in proximity of one another. While the geometries and aspects
1137 of the kinematics of micro-scale fractures may appear similar to those of continental rifts, it
1138 is not yet known if the mathematical solutions for fracture propagation are applicable and
1139 relevant to the scale of rift basins.

1140 Studies in different continental rift settings have highlighted that rift transfer zones,
1141 magmatic focusing, and rift linkage are often collocated (e.g., Aldrich, 1986; Ebinger, 1989;
1142 Nelson et al., 1992; Acocella et al., 1999; Wilson, 1999; Muirhead et al., 2015; Heilman et al.,
1143 2019). However, since the transfer zone breaching faults are relatively younger and often
1144 not as well developed as the major faults of the interacting rift segments, questions remain
1145 on this proposed association. Further, we raise another question on the relationship
1146 between the successful branches of a rift splay and the localization of transfer zone
1147 magmatism. We observe that the higher strain Songwe Trough of the SE Rukwa Rift
1148 bifurcation hosts the Rungwe Volcanic Province (Figure 4a; Heilman et al., 2019), whereas
1149 the Toro Ankole Volcanic Province is in the Lake George Graben of the northern Edward Rift
1150 bifurcation (Figures 4a and 13a). Also, there is a need to better understand the mechanisms
1151 that facilitate magmatic focusing into transfer zones with thick crusts in young continental
1152 rift settings (e.g., lower crustal intrusions in South Tanganyika – Rukwa Transfer Zone;

1153 Hodgson et al., 2017). In addition, there is a need to better understand the absence of
1154 magmatism in breached transfer zones where no surface or deeper magmatism have been
1155 observed (e.g., Albertine - Rhino Rift's Butiaba Transfer Zone). Future studies should also
1156 investigate the influence of short-wavelength dynamic topography on rift transfer zone
1157 evolution.

1158

1159 **Conclusions**

1160 We investigated the stages of early-rift linkage and the associated physiographic,
1161 sedimentation, and structural patterns in the juvenile western Branch of the East African Rift
1162 System. We examine four representative transfer zones in the region and explore the
1163 relationships between the breaching faults, axial drainage patterns, basement structure, and
1164 the extension direction. Our main results are:

1165 1.) A new and broader rift transfer zone classification that encompasses a wider range of
1166 plan-view transfer zone geometries and dip polarity of the interacting border faults.

1167 2.) Although rift transfer zones may differ in both their geometries, and evolutionary stages,
1168 there exist distinct long-wavelength 2-D topographic relief geometries, directionality of axial
1169 stream flow, and breaching fault patterns that characterize rift transfer zones at the various
1170 stages of rift linkage.

1171 3.) These stages include unbreached, partially breached, recently breached, and breached
1172 transfer zones.

1173 4.) At deforming rift transfer zones, breaching may propagate in a single direction i.e.,
1174 unidirectional (distinct propagator and receiver segments), or in a bi-directional manner
1175 (both interacting segments act as propagators and receivers), which may also modulate the
1176 cross-over relief shape.

1177 5.) Depending on the transfer zone geometry, breaching is commonly facilitated by rift-flank
1178 deformation and/or distinct rift-tip structures. Propagating rift-tip structures observed in
1179 the study areas include rift splay, border fault rotation, and fault cluster networks.

1180 6.) The lateral propagation of the transfer zone breaching faults at the rift tips and flanks
1181 (particularly in the absence of magmatism) may be modulated by both the extension
1182 direction and inherited basement structures.

1183 7.) At least 60 % of the rift transfer zones along the western, southwestern, and southeastern
1184 branches of the EARS exhibit breached transfer zone characteristics, indicating the early
1185 linkage of the rift segments. In addition, unbreached and partially breached transfer zones
1186 are largely located in the southern and southwestern parts of the rift system, indicating
1187 continued lateral rift propagation and coalescence to the south and southwest.

1188 Our findings offer a broader insight into the geometrical complexity and structural evolution
1189 of rift transfer zones, and provide first-order predictions of large-scale sedimentation
1190 patterns of humid early-stage continental rift environments. Further, the proposed models
1191 provide testable hypotheses for linking rift architecture and patterns of early-stage
1192 (stretching phase) rift sedimentation applicable to ancient rift basins. However, we
1193 acknowledge that further refinement of these models should be undertaken with additional
1194 studies of both ancient and modern systems.

1195

1196 **Acknowledgements**

1197 We thank the South African Development Community (SADC) for providing the Tanzania
1198 aeromagnetic dataset used in this study. Thanks to Geological Survey of Malawi for providing
1199 the 2013 aeromagnetic datasets used in this study. None of the authors have a conflict of
1200 interest to declare. We also thank the editor Atle Rotevatn, reviewer Jack Williams, and an
1201 anonymous reviewer for their constructive comments that have helped to improve the
1202 quality of the manuscript.

1203

1204 **Data Availability**

1205 The Global Multi-Resolution Topography (GMRT) dataset used in this study is public domain
1206 and is freely available through the GeoMapApp (Ryan et al., 2009). The southern Malawi
1207 Total Magnetic Intensity (TMI) dataset is archived at the Interdisciplinary Earth Data
1208 Alliance (IEDA) at doi:10.1594/IEDA/324860 (Nyalugwe et al., 2019b).

1209 **References**

1210 Aanyu, K. and Koehn, D., 2011. Influence of pre-existing fabrics on fault kinematics and rift
1211 geometry of interacting segments: analogue models based on the Albertine Rift (Uganda),
1212 Western Branch-East African Rift System. *Journal of African Earth Sciences*, 59(2-3), 168-
1213 184.

1214 Acocella, V., Faccenna, C., Funiciello, R. and Rossetti, F., 1999. Sand-box modelling of
1215 basement-controlled transfer zones in extensional domains. *Terra Nova-Oxford*, 11(4),
1216 pp.149-156.

1217 Aldrich, M.J., 1986. Tectonics of the Jemez Lineament in the Jemez Mountains and Rio Grande
1218 Rift. *J. Geophys. Res.* 91, 1753–1762.

1219 Allen, P.A., 2008. From landscapes into geological history. *Nature*, 451(7176), 274-276.

- 1220 Annandale, G.W., 1995. Erodibility. *Journal of hydraulic research*, 33(4), 471-494.
- 1221 Arkani-Hamed, J. (1988). Differential reduction-to-the-pole of regional magnetic anomalies.
1222 *Geophysics*, 53(12), 1592–1600. <https://doi.org/10.1190/1.1442441>.
- 1223 Barnes, J.B., Densmore, A.L., Mukul, M., Sinha, R., Jain, V. and Tandon, S.K., 2011. Interplay
1224 between faulting and base level in the development of Himalayan frontal fold topography.
1225 *Journal of Geophysical Research: Earth Surface*, 116(F3).
- 1226 Behn, M.D., Lin, J., 2000. Segmentation in gravity and magnetic anomalies along the U.S. east
1227 coast passive margin; implications for incipient structure of the oceanic lithosphere. *J.*
1228 *Geophys. Res.* 105 (11), 25769–25790.
- 1229 Bloomfield, K., and Garson, M. S. 1965. The geology of the kirk range – Lisungwe valley area.
1230 *Bulletin of the Geological Survey of Malawi* 17, Government Printer, Zomba.
- 1231 Boone, S.C., Kohn, B.P., Gleadow, A.J., Morley, C.K., Seiler, C. and Foster, D.A., 2019. Birth of
1232 the East African Rift System: Nucleation of magmatism and strain in the Turkana Depression.
1233 *Geology*, 47(9), 886-890.
- 1234 Bosworth, W., 1985. Geometry of propagating continental rifts. *Nature*, 316(6029), 625-627.
- 1235 Braile, L., Keller, G., Wendlandt, R., Morgan, P., & Khan, M. (2006). Chapter 5 The east african
1236 rift system. *Continental Rifts: Evolution, Structure, Tectonics Developments in Geotectonics*.
- 1237 Childs, C., Holdsworth, R. E., Jackson, C. A.-L., Manzocchi, T., Walsh, J. J. & Yielding, G. (eds)
1238 2017. *The Geometry and Growth of Normal Faults*. Geological Society, London, Special
1239 Publications, 439, 79–107.
- 1240 Choubert, G., Faure-Muret, A., Chanteux, P., Roche, G., Simpson, E.S.W., Shackleton, L.,
1241 Ségoufin, J., Seguin, C. and Sougy, J., 1988. International geological map of Africa. Scale 1: 5
1242 000 000, Commission for the Geological Map of the World (CGMW), Unesco, Paris.
- 1243 Cochran, J.R., Martinez, F., 1988. Evidence from the northern Red Sea on the transition from
1244 continental to oceanic rifting. *Tectonophysics* 153 (1–4), 25–53.
- 1245 Cohen, A. S., Boclaer, B. V., Todd, J. A., Mcglue, M., Michel, E., Nkotagu, H. H., ... Delvaux, D.
1246 (2013). Quaternary ostracodes and molluscs from the Rukwa Basin (Tanzania) and their
1247 evolutionary and paleobiogeographic implications. *Palaeogeography, Palaeoclimatology,*
1248 *Palaeoecology*, 392, 79–97.
- 1249 Collanega, L., Corti, G., Breda, A., Massironi, M. and Keir, D., 2020. 3D Extension at Plate
1250 Boundaries Accommodated by Interacting Fault Systems. *Scientific Reports*, 10(1), 1-12.
- 1251 Corti, G. (2012). Evolution and characteristics of continental rifting: Analog modeling-
1252 inspired view and comparison with examples from the East African Rift System.
1253 *Tectonophysics*, 522, 1–33.
- 1254 Corti, G., Cioni, R., Franceschini, Z., Sani, F., Scaillet, S., Molin, P., Isola, I., Mazzarini, F., Brune,
1255 S., Keir, D. and Erbello, A., 2019. Aborted propagation of the Ethiopian rift caused by linkage
1256 with the Kenyan rift. *Nature communications*, 10(1), 1-11.

- 1257 Cowie, P.A., Underhill, J.R., Behn, M.D., Lin, J. and Gill, C.E., 2005. Spatio-temporal evolution of
1258 strain accumulation derived from multi-scale observations of Late Jurassic rifting in the
1259 northern North Sea: A critical test of models for lithospheric extension. *Earth and Planetary
1260 Science Letters*, 234(3-4), 401-419.
- 1261 Daly, M.C., Chorowicz, J. and Fairhead, J.D., 1989. Rift basin evolution in Africa: the influence
1262 of reactivated steep basement shear zones. *Geological Society, London, Special Publications*,
1263 44(1), 309-334.
- 1264 Daly, M.C., Green, P., Watts, A.B., Davies, O., Chibesakunda, F. and Walker, R., 2020. Tectonics
1265 and Landscape of the Central African Plateau, and their implications for a propagating
1266 Southwestern Rift in Africa. *Geochemistry, Geophysics, Geosystems*, 21, p.e2019GC008746.
- 1267 Delvaux, D., 1989. The Karoo to Recent rifting in the western branch of the East-African Rift
1268 System: A bibliographical synthesis. *Mus. roy. Afr. centr., Tervuren (Belg.), Dépt. Géol. Min.,
1269 Rapp. ann, 1990 (1991)*, 63-83.
- 1270 Delvaux, D., Kervyn, F., Vittori, E., Kajara, R.S.A. and Kilembe, E., 1998. Late Quaternary
1271 tectonic activity and lake level change in the Rukwa Rift Basin. *Journal of African Earth
1272 Sciences*, 26(3), pp.397-421.
- 1273 Delvaux, D., Kervyn, F., Macheyeke, A. S., & Temu, E. B. (2012). Geodynamic significance of the
1274 TRM segment in the East African Rift (W - Tanzania): Active tectonics and paleostress in the
1275 Ufipa plateau and Rukwa basin. *Journal of Structural Geology*, 37, 161–180.
1276 <https://doi.org/10.1016/j.jsg.2012.01.008>
- 1277 Dèzes, P., Schmid, S.M. and Ziegler, P.A., 2004. Evolution of the European Cenozoic Rift
1278 System: interaction of the Alpine and Pyrenean orogens with their foreland lithosphere.
1279 *Tectonophysics*, 389(1-2), 1-33.
- 1280 Drury, S. A. (2001). *Image interpretation in geology*, 3rd Edition, Blackwell Science Inc.,
1281 Malden, MA.
- 1282 Dulanya, Z., 2017. A review of the geomorphotectonic evolution of the south Malawi rift.
1283 *Journal of African Earth Sciences*, 129, pp.728-738.
- 1284 Ebinger, C.J., 1989. Tectonic development of the western branch of the East African rift
1285 system. *Geol. Soc. Am. Bull.* 101, 885e903
- 1286 Ebinger, C. (2012). Evolution of the Cenozoic East African rift system. *Regional Geology and
1287 Tectonics: Phanerozoic Rift Systems and Sedimentary Basins*, 132–162.
- 1288 Emishaw, L. and Abdelsalam, M.G., 2019. Development of Late Jurassic - Early Paleogene and
1289 Neogene - Quaternary Rifts Within the Turkana Depression, East Africa From Satellite
1290 Gravity Data. *Tectonics*, 38(7), 2358-2377.
- 1291 Fairhead, J.D., 1988. Mesozoic plate tectonic reconstructions of the central South Atlantic
1292 Ocean: the role of the West and Central African rift system. *Tectonophysics*, 155(1-4), 181-
1293 191.

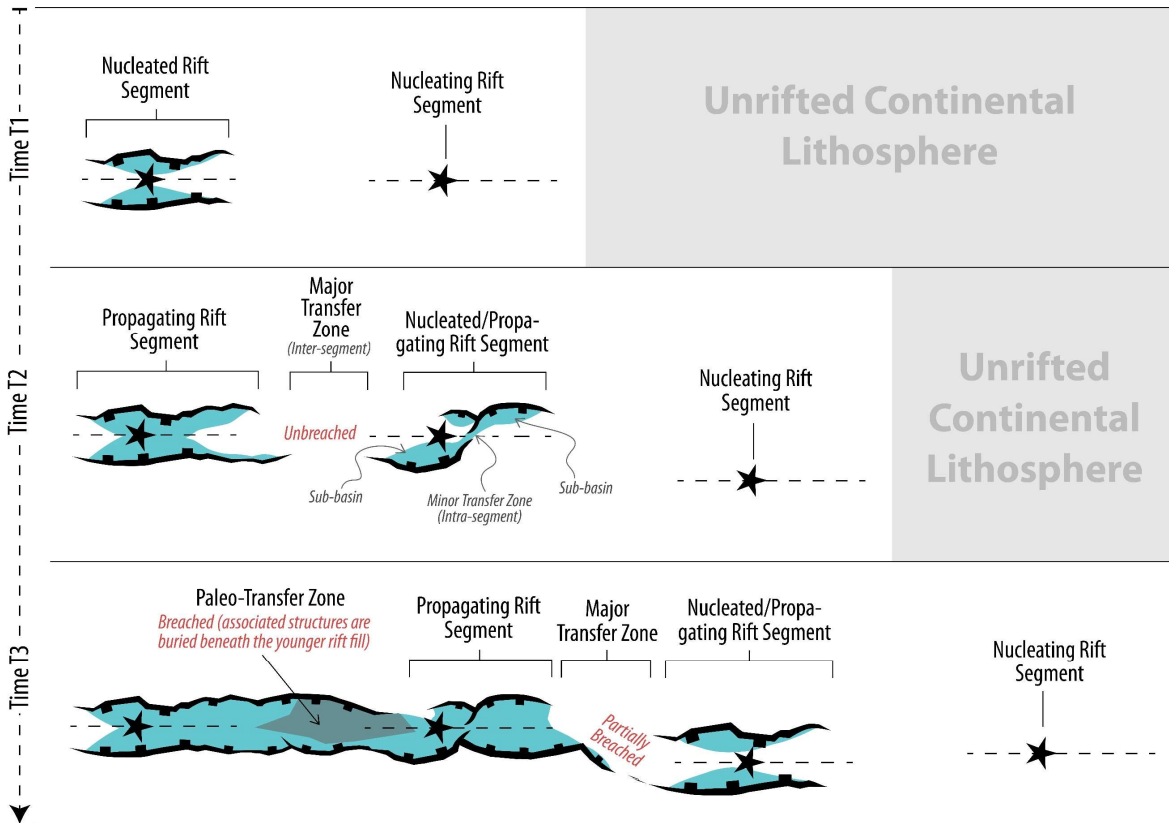
- 1294 Fritz, H., Abdelsalam, M., Ali, K. A., Bingen, B., Collins, A. S., Fowler, A. R., et al. (2013). Orogen
1295 styles in the East African Orogen: A review of the Neoproterozoic to Cambrian tectonic
1296 evolution. *Journal of African Earth Sciences*, 86, 65–106.
- 1297 Gawthorpe, R.L. and Leeder, M.R., 2000. Tectono-sedimentary evolution of active extensional
1298 basins. *Basin Research*, 12(3-4), 195-218.
- 1299 Gupta, S., Cowie, P.A., Dawers, N.H. and Underhill, J.R., 1998. A mechanism to explain rift-
1300 basin subsidence and stratigraphic patterns through fault-array evolution. *Geology*, 26(7),
1301 pp.595-598.
- 1302 GTK Consortium (2012), Explanation of the geology of sheets NA-36-1 and NA-36-5 (Arua
1303 and Pakwach) 1:250,000, Uganda. Department of Geological Survey and Mines (DGSM),
1304 Entebbe. 115p.
- 1305 Hans Nelson, C., Karabanov, E.B., Colman, S.M. and Escutia, C., 1999. Tectonic and sediment
1306 supply control of deep rift lake turbidite systems: Lake Baikal, Russia. *Geology*, 27(2),
1307 pp.163-166.
- 1308 Heron, P.J., Peace, A.L., McCaffrey, K.J.W., Welford, J.K., Wilson, R., van Hunen, J. and
1309 Pysklywec, R.N., 2019. Segmentation of rifts through structural inheritance: Creation of the
1310 Davis Strait. *Tectonics*, 38(7), pp.2411-2430.
- 1311 Hodgson, I., Illsley - Kemp, F., Gallacher, R. J., Keir, D., Ebinger, C. J., & Mtelela, K. (2017).
1312 Crustal structure at a young continental rift: A receiver function study from the Tanganyika
1313 Rift. *Tectonics*, 36, 2806–2822.
- 1314 Hovius, N. (1998). Controls on sediment supply by large rivers. In: *Relative role of eustasy,
1315 climate and tectonism in continental rocks: Tulsa, Oklahoma.* (Ed. By Shanley, K.W. &
1316 McCabe, P. J). SEPM Special Publication, 59, 2–16.
- 1317 Jackson, C.A.L., Gawthorpe, R.L., Carr, I.D. and Sharp, I.R., 2005. Normal faulting as a control
1318 on the stratigraphic development of shallow marine syn-rift sequences: the Nukhul and
1319 Lower Rudeis Formations, Hammam Faraun fault block, Suez Rift, Egypt. *Sedimentology*,
1320 52(2), pp.313-338.
- 1321 Katumwehe, A.B., Abdelsalam, M.G. and Atekwana, E.A., 2015. The role of pre-existing
1322 Precambrian structures in rift evolution: The Albertine and Rhino grabens, Uganda.
1323 *Tectonophysics*, 646, pp.117-129.
- 1324 Katumwehe, A.B., Abdelsalam, M.G., Atekwana, E.A. and Laó-Dávila, D.A., 2016. Extent,
1325 kinematics and tectonic origin of the Precambrian Aswa Shear Zone in eastern Africa.
1326 *Gondwana Research*, 34, pp.241-253.
- 1327 Kim, Y.S., Peacock, D.C. and Sanderson, D.J., 2004. Fault damage zones. *Journal of structural
1328 geology*, 26(3), pp.503-517.
- 1329 Koehn, D., Aanyu, K., Haines, S. and Sachau, T., 2008. Rift nucleation, rift propagation and the
1330 creation of basement micro-plates within active rifts. *Tectonophysics*, 458(1-4), 105-116.

- 1331 Kolawole, F., Atekwana, E.A., Laó-Dávila, D.A., Abdelsalam, M.G., Chindandali, P.R., Salima, J.
 1332 and Kalindekafe, L., 2018. Active deformation of Malawi rift's north basin Hinge zone
 1333 modulated by reactivation of preexisting Precambrian Shear zone fabric. *Tectonics*, 37(3),
 1334 pp.683-704.
- 1335 Lambiase, J.J. and Bosworth, W., 1995. Structural controls on sedimentation in continental
 1336 rifts. *Geological Society, London, Special Publications*, 80(1), 117-144.
- 1337 La Rosa, A., Pagli, C., Keir, D., Sani, F., Corti, G., Wang, H. and Possee, D., 2019. Observing
 1338 Oblique Slip During Rift Linkage in Northern Afar. *Geophysical Research Letters*, 46(19),
 1339 10782-10790.
- 1340 Lavayssière, A. J., Drooff, C. J., Ebinger, C. J., Gallacher, R. J., Illsley-Kemp, F. J., Oliva, S. J., &
 1341 Keir, D. J. (2019). Depth Extent and Kinematics of Faulting in the Southern Tanganyika Rift,
 1342 Africa. *Tectonics*, 38(3), 842–862. doi: 10.1029/2018tc005379.
- 1343 Lazarus, E. D., and Constantine, J. A. (2013). Generic theory for channel sinuosity.
 1344 *Proceedings of the National Academy of Sciences*, 110(21), pp.8447-8452.
- 1345 Lyons, R. P., Scholz, C. A., Cohen, A. S., King, J. W., Brown, E. T., Ivory, S. J., et al. (2015).
 1346 Continuous 1.3-million-year record of East African hydroclimate, and implications for
 1347 patterns of evolution and biodiversity. *Proceedings of the National Academy of Sciences of*
 1348 *the United States of America*, 112(51), 15,568-15,573.
- 1349 Ma, G. Q., Du, X. J., Li, L. L., & Meng, L. S. (2012). Interpretation of magnetic anomalies by
 1350 horizontal and vertical derivatives of the analytic signal. *Applied Geophysics*, 9(4), 468–474.
 1351 <https://doi.org/10.1007/s11770-012-0350-4>.
- 1352 Mack, G.H., Seager, W.R., Leeder, M.R., Perez-Arlucea, M. and Salyards, S.L., 2006. Pliocene
 1353 and Quaternary history of the Rio Grande, the axial river of the southern Rio Grande rift, New
 1354 Mexico, USA. *Earth-Science Reviews*, 79(1-2), pp.141-162.
- 1355 Mardia, K. V., and Jupp, P. E., 2009. *Directional statistics*. Vol. 494, John Wiley & Sons, West
 1356 Sussex, England.
- 1357 Morley, C.K., 2020. Early syn-rift igneous dike patterns, northern Kenya Rift (Turkana,
 1358 Kenya): Implications for local and regional stresses, tectonics, and magma-structure
 1359 interactions. *Geosphere*, 16(3), 890-918.
- 1360 Muirhead, J.D., Kattenhorn, S.A. and Le Corvec, N., 2015. Varying styles of magmatic strain
 1361 accommodation across the East African Rift. *Geochemistry, Geophysics, Geosystems*, 16(8),
 1362 pp.2775-2795.
- 1363 Morley, C.K., Nelson, R.A., Patton, T.L. and Munn, S.G., 1990. Transfer zones in the East African
 1364 rift system and their relevance to hydrocarbon exploration in rifts. *AAPG bulletin*, 74(8),
 1365 1234-1253.
- 1366 Morley, C. K., Cunningham, S. M., Harper, R. M. and Wescott, W. A. (1992). Geology and
 1367 geophysics of the Rukwa rift, East Africa. *Tectonics*, 11(1), pp.69-81.

- 1368 Muirhead, J. D., Wright, L. J., & Scholz, C. A. (2019). Rift evolution in regions of low magma
1369 input in East Africa. *Earth and Planetary Science Letters*, 506, 332–346.
- 1370 Nelson, R.A., Patton, T.L. and Morley, C.K., 1992. Rift-segment interaction and its relation to
1371 hydrocarbon exploration in continental rift systems (1). *AAPG bulletin*, 76(8), pp.1153-1169.
- 1372 Ngalamo, J.F.G., Kolawole, F., Sobh, M. and Atekwana, E.A. (2020). Partitioning of Extension
1373 at the Propagating Tips of Continental Rifts: Insights from the Central and East African Rift
1374 Systems. *AGU Fall Meeting Abstract #T028-06*.
- 1375 Nyalugwe, V.N., Abdelsalam, M.G., Atekwana, E.A., Katumwehe, A., Mickus, K.L., Salima, J.,
1376 Njinju, E.A. and Emishaw, L., (2019a). Lithospheric structure beneath the Cretaceous Chilwa
1377 Alkaline Province (CAP) in southern Malawi and northeastern Mozambique. *Journal of*
1378 *Geophysical Research: Solid Earth*, 124(11), pp.12224-12240.
- 1379 Nyalugwe, V.; Abdelsalam, M.; Atekwana, E.; Katumwehe, A.; Mickus, K.; Salima, J.; Njinju, E.
1380 and L. Emishaw, (2019b). 2013 Total Magnetic Intensity (TMI) gridded aeromagnetic data
1381 of southern Malawi 34 45 E – 36 00 E and 14 45 S and 16 15 S (investigator Mohamed
1382 Abdelsalam). *Integrated Earth Data Applications (IEDA)*. doi:10.1594/IEDA/324860.
- 1383 Nyalugwe, V.N., Abdelsalam, M.G., Katumwehe, A., Mickus, K.L. and Atekwana, E.A., 2020.
1384 Structure and tectonic setting of the Chingale Igneous Ring Complex, Malawi from
1385 aeromagnetic and satellite gravity data: Implication for Precambrian terranes collision and
1386 Neogene-Quaternary rifting. *Journal of African Earth Sciences*, 163, p.103760.
- 1387 Pagli, C., Yun, S.H., Ebinger, C., Keir, D. and Wang, H., 2019. Strike-slip tectonics during rift
1388 linkage. *Geology*, 47(1), pp.31-34.
- 1389 Perrin, C., Manighetti, I. and Gaudemer, Y., 2016. Off-fault tip splay networks: A genetic and
1390 generic property of faults indicative of their long-term propagation. *Comptes Rendus*
1391 *Geoscience*, 348(1), pp.52-60.
- 1392 Phillips, T.B. and McCaffrey, K.J., 2019. Terrane Boundary Reactivation, Barriers to Lateral
1393 Fault Propagation and Reactivated Fabrics: Rifting Across the Median Batholith Zone, Great
1394 South Basin, New Zealand. *Tectonics*, 38(11), pp.4027-4053.
- 1395 Ring, U., 1995. Tectonic and lithological constraints on the evolution of the Karoo graben of
1396 northern Malawi (East Africa). *Geologische Rundschau*, 84(3), 607-625.
- 1397 Roberts, E.M., Stevens, N.J., O'Connor, P.M., Dirks, P.H.G.M., Gottfried, M.D., Clyde, W.C.,
1398 Armstrong, R.A., Kemp, A.I.S. and Hemming, S., 2012. Initiation of the western branch of the
1399 East African Rift coeval with the eastern branch. *Nature Geoscience*, 5(4), pp.289-294.
- 1400 Rotevatn, A., Kristensen, T.B., Ksienzyk, A.K., Wemmer, K., Henstra, G.A., Midtkandal, I.,
1401 Grundvåg, S.A. and Andresen, A., 2018. Structural inheritance and rapid rift-length
1402 establishment in a multiphase rift: The East Greenland rift system and its Caledonian
1403 orogenic ancestry. *Tectonics*, 37(6), pp.1858-1875.
- 1404 Ryan, W. B. F., S.M. Carbotte, J. Coplan, S. O'Hara, A. Melkonian, R. Arko, R.A. Weissel, V.
1405 Ferrini, A. Goodwillie, F. Nitsche, J. Bonczkowski, and R. Zemsky (2009), *Global Multi-*
1406 *Resolution Topography (GMRT) synthesis data set, *Geochem. Geophys. Geosyst.*, 10, Q03014.*

- 1407 Roberts, E.M., Stevens, N.J., O'Connor, P.M., Dirks, P.H.G.M., Gottfried, M.D., Clyde, W.C.,
 1408 Armstrong, R.A., Kemp, A.I.S. and Hemming, S., 2012. Initiation of the western branch of the
 1409 East African Rift coeval with the eastern branch. *Nature Geoscience*, 5(4), pp.289-294.
- 1410 Saria, E., Calais, E., Stamps, D.S., Delvaux, D. and Hartnady, C.J.H., 2014. Present-day
 1411 kinematics of the East African Rift. *Journal of Geophysical Research: Solid Earth*, 119(4),
 1412 pp.3584-3600.
- 1413 Simon, B., Guillocheau, F., Robin, C., Dauteuil, O., Nalpas, T., Pickford, M., Senut, B., Lays, P.,
 1414 Bourges, P. and Bez, M., 2017. Deformation and sedimentary evolution of the Lake Albert Rift
 1415 (Uganda, East African rift system). *Marine and Petroleum Geology*, 86, pp.17-37.
- 1416 Scholz, C.A., Shillington, D.J., Wright, L.J., Accardo, N., Gaherty, J.B. and Chindandali, P., 2020.
 1417 Intrarift fault fabric, segmentation, and basin evolution of the Lake Malawi (Nyasa) Rift, East
 1418 Africa. *Geosphere*, 16(5), 1293-1311.
- 1419 Soreghan, M.J. and Cohen, A.S., 1996. Textural and compositional variability across littoral
 1420 segments of Lake Tanganyika: the effect of asymmetric basin structure on sedimentation in
 1421 large rift lakes. *AAPG bulletin*, 80(3), pp.382-408.
- 1422 Soreghan, M.J., Scholz, C.A. and Wells, J.T., 1999. Coarse-grained, deep-water sedimentation
 1423 along a border fault margin of Lake Malawi, Africa; seismic stratigraphic analysis. *Journal of*
 1424 *Sedimentary Research*, 69(4), pp.832-846.
- 1425 Specht, T.D. and Rosendahl, B.R., 1989. Architecture of the Lake Malawi rift, east Africa.
 1426 *Journal of African Earth Sciences (and the Middle East)*, 8(2-4), pp.355-382.
- 1427 Taylor, S.K., Bull, J.M., Lamarche, G. and Barnes, P.M., 2004. Normal fault growth and linkage
 1428 in the Whakatane Graben, New Zealand, during the last 1.3 Myr. *Journal of Geophysical*
 1429 *Research: Solid Earth*, 109(B2).
- 1430 Thomas D. S. G., Bailey, R., Shaw, P. A., Durcan, J. A., & Singarayer, J. S. (2009). Late
 1431 Quaternary highstands at Lake Chilwa, Malawi: Frequency, timing and possible forcing
 1432 mechanisms in the last 44 ka. *Quaternary Science Reviews*, 28, 526–539.
- 1433 Tiercelin, J.J., Soreghan, M., Cohen, A.S., Lezzar, K.E. and Bouroulllec, J.L., 1992. Sedimentation
 1434 in large rift lakes: example from the Middle Pleistocene—Modern deposits of the Tanganyika
 1435 Trough, East African Rift System. *Bull. Centres Rech. Explor.-Prod. Elf Aquitaine*, 16, pp.83-
 1436 111.
- 1437 Vittori, E., Delvaux, D. and Kervyn, F., 1997. Kanda fault: A major seismogenic element west
 1438 of the Rukwa Rift (Tanzania, East Africa). *Journal of Geodynamics*, 24(1-4), pp.139-153.
- 1439 Wedmore, L., Biggs, J., Williams, J., Fagereng, A., Dulanya, Z., Mphepo, F. and Mdala, H. (2020).
 1440 Active fault scarps in southern Malawi and their implications for the distribution of strain in
 1441 incipient continental rifts. *Tectonics*, 39, e2019TC005834.
- 1442 Westerhof, A.B., Härmä, P., Isabirye, E., Katto, E., Koistinen, T., Kuosmanen, E., Lehto, T.,
 1443 Lehtonen, M.I., Mäkitie, H., Manninen, T. and Mänttari, I. (2014). Geology and geodynamic
 1444 development of Uganda with explanation of the 1:1,000,000 scale geological map. Geological
 1445 survey of Finland.

- 1446 Williams, J.N., Fagereng, Å., Wedmore, L.N., Biggs, J., Mphepo, F., Dulanya, Z., Mdala, H. and
1447 Blenkinsop, T., 2019. How do variably striking faults reactivate during rifting? Insights from
1448 southern Malawi. *Geochemistry, Geophysics, Geosystems*, 20(7), pp.3588-3607.
- 1449 Wilson, T.J., 1999. Cenozoic structural segmentation of the Transantarctic Mountains rift
1450 flank in southern Victoria Land. *Global and Planetary Change*, 23(1-4), 105-127.
- 1451 Woolley, A.R., 2001. *Alkaline Rocks and Carbonatites of the World. Part 3: Africa*. The
1452 Geological Society, London, p. 372.
- 1453 Wright, L.J., Muirhead, J.D. and Scholz, C.A., 2020. Spatio-temporal variations in upper crustal
1454 extension across the different basement terranes of the Lake Tanganyika Rift, East Africa.
1455 *Tectonics*.
- 1456 Zondervan, J.R., Stokes, M., Boulton, S.J., Telfer, M.W. and Mather, A.E., 2020. Rock strength
1457 and structural controls on fluvial erodibility: Implications for drainage divide mobility in a
1458 collisional mountain belt. *Earth and Planetary Science Letters*, 538, p.116221.
- 1459 Zwaan, F., Schreurs, G., Naliboff, J., & Buitert, S. J. (2016). Insights into the effects of oblique
1460 extension on continental rift interaction from 3D analogue and numerical models.
1461 *Tectonophysics*, 693, 239–260.
- 1462
- 1463
- 1464
- 1465



1467 **Figure 1:** Simple model of nucleation and growth of rift segments along continental rift
 1468 systems (modified after Nelson et al., 1992). Rift axes are represented by the black
 1469 stars/dashed lines. Note that this cartoon only features collinear and underlapping parallel
 1470 rift segments. Also, note that for each transfer zone, the cartoon illustrates the pre- and post-
 1471 linkage geometries of the rift zones.

1472

1473

1474

1475

1476

1477

1478

1479

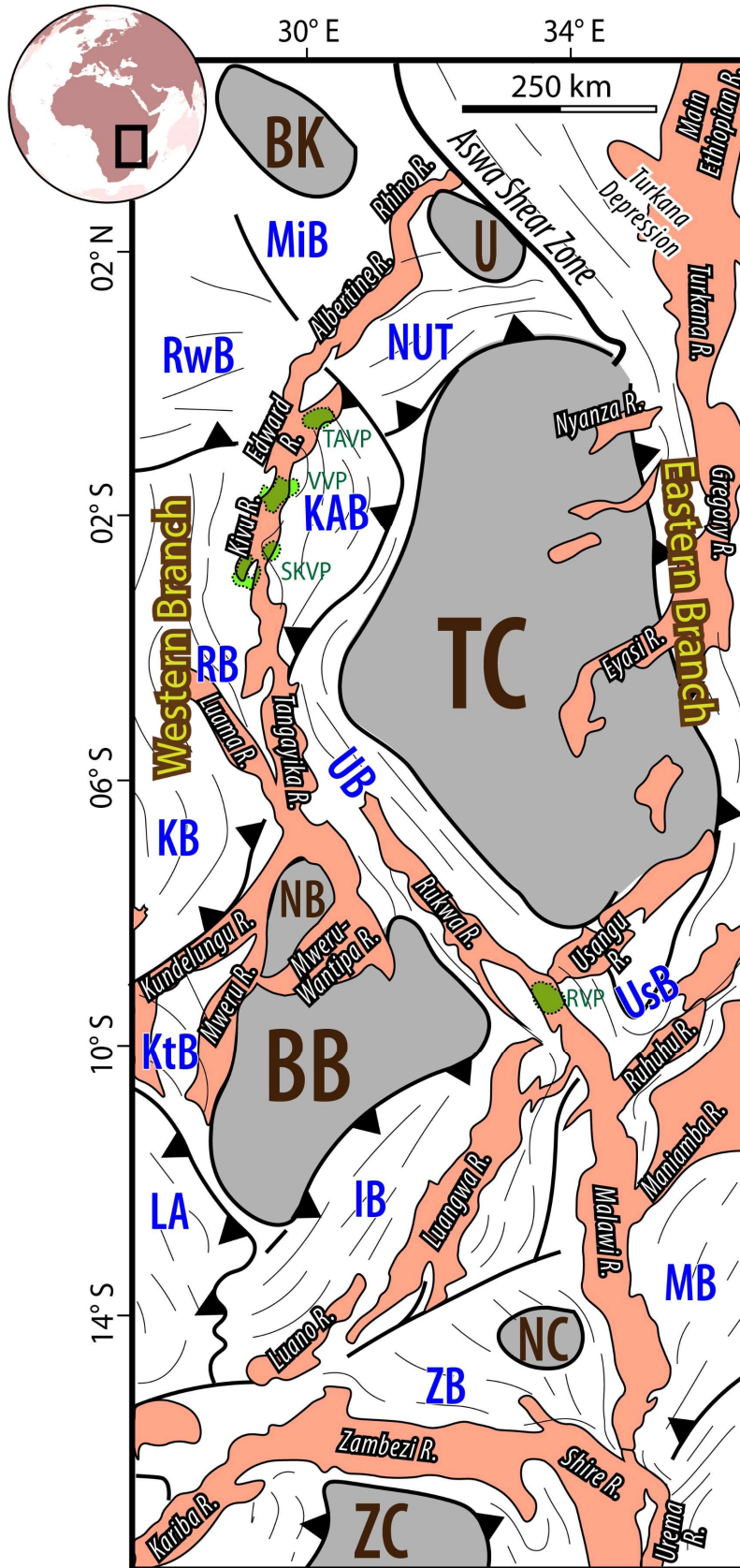
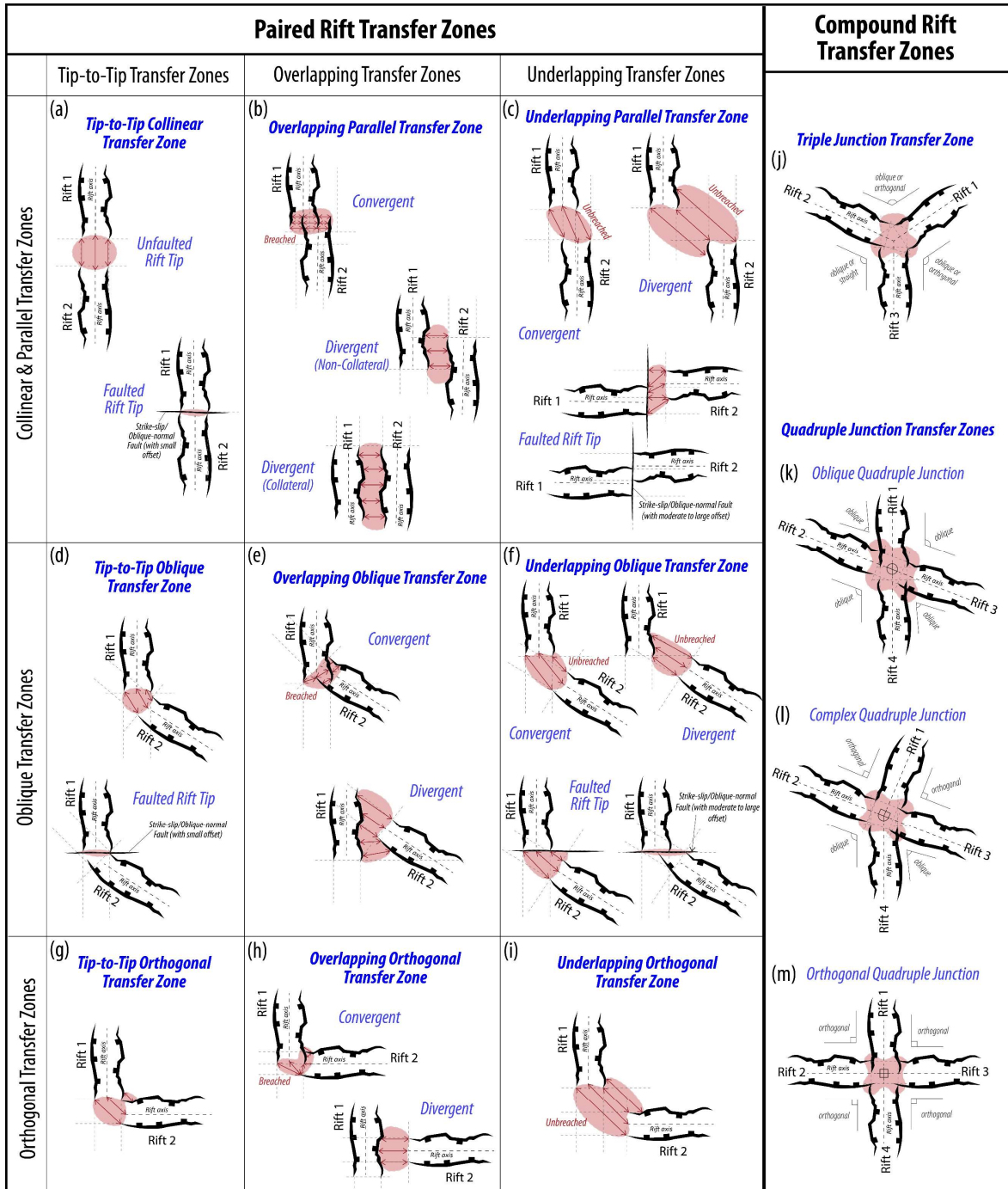


Figure 2: Map of eastern Africa showing the Precambrian basement orogenic belts with their large-scale fabric trends, cratonic blocks (grey), and rift basins (pink; includes both Mesozoic and Cenozoic rifts) modified after Daly et al. (1989). The cratons include the BB (Bangweulu Block), BK (Bomu-Kibalia Block), NC (Niassa Craton), TC (Tanzanian Craton), U (Uganda Craton), and ZC (Zimbabwe Craton). The mobile belts include IB (Irumide Belt), KAB (Karagwe-Ankole Belt), KB (Kibaran Belt), KtB (Katangan Belt), LA (Lufillian Arc), MB (Mozambique Belt), MiB (Madi-Igisi Belt), NB (North Bangweulu Microplate), NUT (North Uganda Terrane), RB (Ruzizian Belt), RWB (Ruwendori Belt), UB (Ubendian Belt), UsB (Usagaran Belt), ZB (Zambezi Belt). Active volcanic centers along the Western Branch of the East African Rift System (green polygons) are RVP (Rungwe Volcanic Province), SKVP (South Kivu Volcanic Province), TAVP (Toro-Ankole Volcanic Province), VVP (Virunga Volcanic Province).

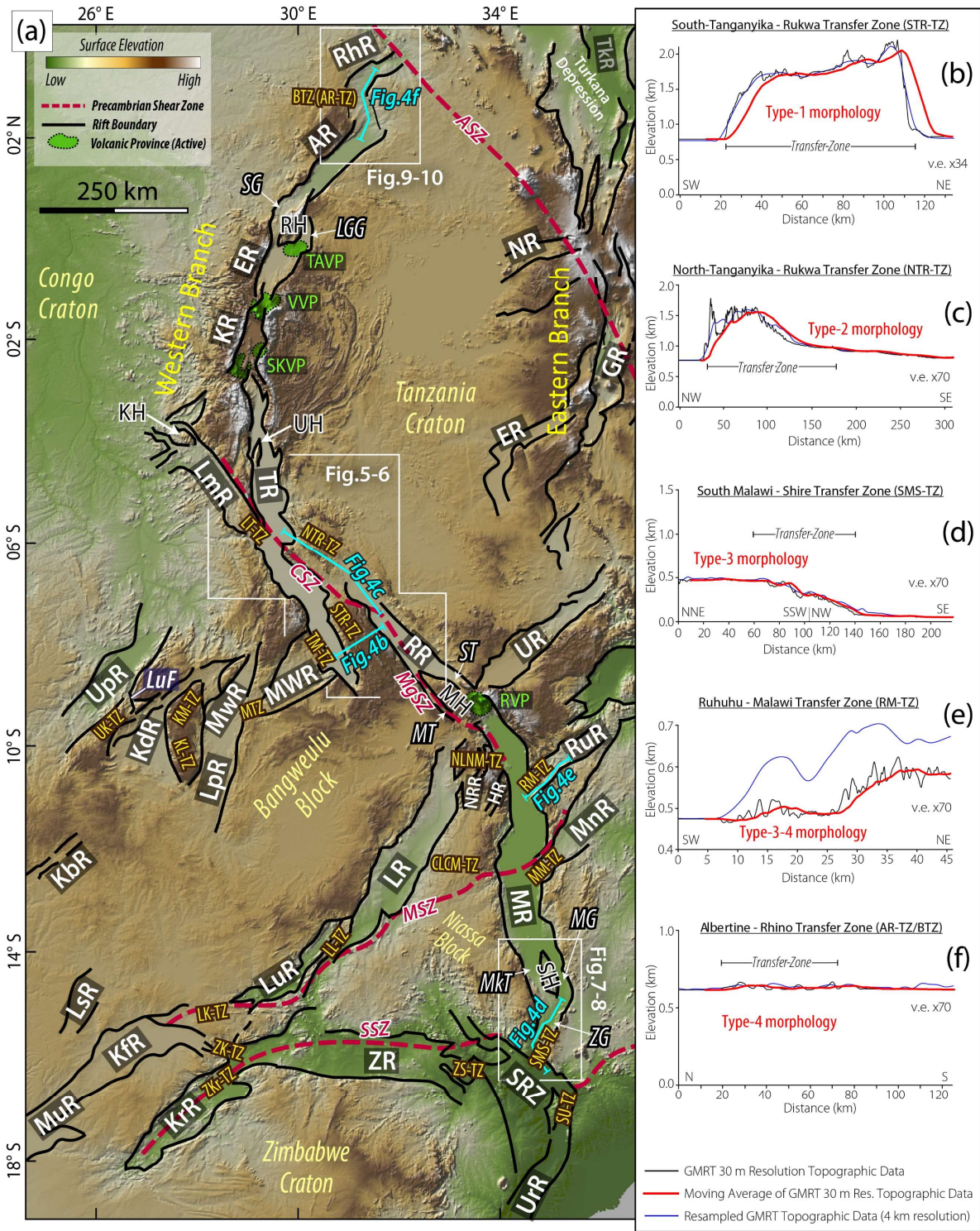
1520
1521
1522
1523
1524
1525
1526
1527
1528
1529
1530
1531
1532
1533
1534
1535
1536
1537
1538
1539
1540



 **Rift-bounding fault**
  **Rift Transfer Zone: Cross-over region between interacting rift segments, across which breaching faults may develop.**
  **Breaching Distance: Lateral extents between the primary structural domains of the interacting rifts (border fault & intrabasin zones).**

1541 **Figure 3:** Broader classification of rift transfer zones. This updated classification is based on
 1542 a review of previously published classifications (Morley et al., 1990; Nelson et al., 1992),
 1543 other geometries observable in the East African Rift System and several other continental
 1544 rift systems. Note that the rift segments, although presented as grabens, can also be half-
 1545 grabens. The faults shown are basin-bounding fault systems.

1546
1547
1548
1549
1550
1551
1552
1553
1554
1555
1556
1557
1558
1559
1560
1561
1562
1563
1564
1565
1566
1567



1568 **Figure 4: Eastern Africa rift basins and the major transfer zones.** (a) Map of eastern Africa
 1569 showing the different segments of the Cenozoic western (WB-EARS) of the East African Rift
 1570 System (and some of the Eastern branch segments). Also shown are the Mesozoic rift
 1571 segments that are reactivated (e.g., LR, RR, SRZ) and unreactivated (e.g., LmR, MnR, RuR, ZR)
 1572 during the Cenozoic extension. AR: Albertine Rift, BTZ (AR-TZ): Butiaba Transfer Zone

1573 (Albertine-Rhino TZ), CSZ: Chisi Suture Zone, CLCM-TZ: Central Luangwa-Central Malawi
1574 Transfer Zone, ER: Eyasi Rift, GR: Gregory Rift, HR: Henga Rift, KbR: Kabompo Rift, KdR:
1575 Kundelungu Rift, KfR: Kafue Rift, KH: Kabumbi Horst, KL-TZ: Kundelungu-Luapula Transfer
1576 Zone, KM-TZ: Kundelungu-Mweru Transfer Zone, KR: Kivu Rift, Kr: Kariba Rift, LGG: Lake
1577 George Graben, LK-TZ: Luano-Kafue Transfer Zone, LL-TZ: Luangwa-Luano Transfer Zone,
1578 LpR: Luapula Rift, LsR: Luansanza Rift, LT-TZ: Luama-Tanganyika Transfer Zone, LuF: Lufira
1579 Fault, LuR: Luano Rift, LR: Luangwa Rift, LmR: Luama Rift, MG: Malombe Graben, MgSZ:
1580 Mughesse Shear Zone, MH: Mbozi Horst, Mkt: Makanjira Trough, MM-TZ: Maniamba-Malawi
1581 Transfer Zone, MnR: Maniamba Rift, MR: Malawi Rift, MSZ: Mwembeshi Shear Zone, MT:
1582 Musangano Trough, MTZ: Mweru Wantipa Transfer Zone, MuR: Muchili Rift, MWR: Mweru
1583 Rift, MWR: Mweru-Wantipa Rift, NLNM-TZ: North Luangwa-North Malawi Transfer Zone,
1584 NR: Nyanza Rift, NRR: North Rukuru-Mwesia Rift, NTR-TZ: North Tanganyika-Rukwa
1585 Transfer Zone, RH: Rwenzori Horst, RhR: Rhino Rift, RM-TZ: Ruhuhu-Malawi Transfer Zone,
1586 RR: Rukwa Rift, RuR: Ruhuhu Rift, RVP: Rungwe Volcanic Province, SG: Semiliki Graben, SH:
1587 Shire Horst, SKVP: South Kivu Volcanic Province, SMS-TZ: South Malawi-Shire Transfer Zone,
1588 SRZ: Shire Rift Zone, SSZ: Sanangoè Shear Zone, ST: Songwe Trough, STR-TZ: South
1589 Tanganyika-Rukwa Transfer Zone, SU-TZ: Shire-Urema Transfer Zone, TkR: Turkana Rift,
1590 TM-TZ: Tanganyika-Mweru Wantipa Transfer Zone, TR: Tanganyika Rift, TAVP: Toro-Ankole
1591 Volcanic Province, UH: Ubwari Horst, UK-TZ: Upemba-Kundelungu Transfer Zone
1592 (Kundelungu Horst), UpR: Upemba Rift, UR: Usangu Rift, UrR: Urema Rift, VVP: Virunga
1593 Volcanic Province, ZK-TZ: Zambezi-Kafue Transfer Zone, ZKr-TZ: Zambezi-Kariba Transfer
1594 Zone, ZS-TZ: Zambezi-Shire Transfer Zone, ZR: Zambezi Rift. Map Source: Global Multi-
1595 Resolution Topography (GMRT) digital elevation model (Ryan et al., 2009). (b – f) GMRT
1596 Topographic profiles across some of the non-magmatic WB-EARS transfer zones,
1597 highlighting the major categories of long-wavelength cross-over relief geometries (red
1598 curves) that are observed.

1599

1600

1601

1602

1603

1604

1605

1606

1607

1608

1609
 1610
 1611
 1612
 1613
 1614
 1615
 1616
 1617
 1618
 1619
 1620
 1621
 1622
 1623
 1624
 1625
 1626
 1627
 1628
 1629
 1630
 1631
 1632
 1633
 1634
 1635
 1636
 1637
 1638
 1639
 1640
 1641
 1642
 1643
 1644
 1645
 1646
 1647
 1648
 1649
 1650
 1651
 1652

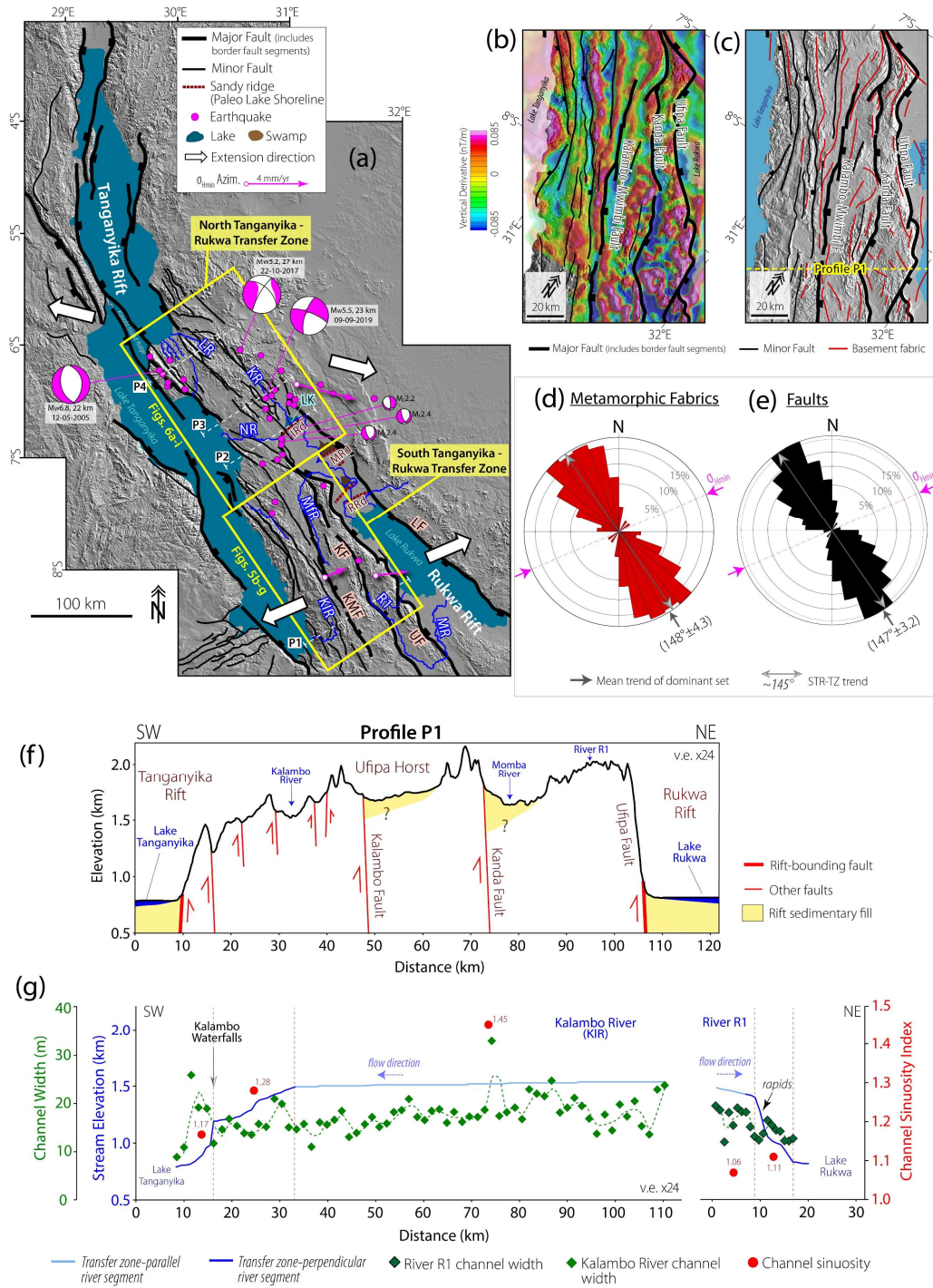


Figure 5: South Tanganyika-Rukwa Transfer Zone, STR-TZ (Parallel Overlapping Divergent). (a.) Satellite Digital Elevation Model (DEM) hillshade map of the Tanganyika Rift and the Rukwa Rift. Earthquake epicenters (Mw3.7 - 7.3) and focal mechanism solutions are from USGS and Global CMT catalogs, and Lavayssiere et al. (2019). Crustal stretching velocity (green arrows) with 95% uncertainty ellipses are from Stamps et al. (2018). IRd = Ilyandi Ridge, KF = Kanda Fault System, KIR = Kalambo River, KMF = Kalambo-Mwimbi Fault System,

1653 KR = Kavuu River, LF = Lupa Fault, LK = Lake Katavi, LR = Luegele River, MfR = Mfuizi River,
1654 MR = Momba River, MRd = Maimba Ridge, NR = Nkamba River, RRd = Rungwa Ridge, UF =
1655 Ufipa Fault. Locations of the paleo-lake shore ridges are from Delvaux et al. (1998).
1656 Tanganyika Rift faults are from Muirhead et al. (2018). (b) Filtered aeromagnetic grid of the
1657 STR-TZ, overlaid on the hillshade DEM showing the magnetic fabrics of the basement. (c)
1658 Satellite DEM hillshade map overlaid with interpretation of the interpreted basement
1659 fabrics. (d) Frequency-azimuth distribution of the aeromagnetic basement fabrics in Figure
1660 3c. (e) Frequency-azimuth distribution of the mapped faults along the transfer zone (Figure
1661 3c). (f) Rift-orthogonal topographic profile across the transfer zone. (g) Longitudinal stream
1662 profiles for representative axial streams in the transfer zone (Kalambo River and an
1663 unnamed river R1).

1664
1665

1666

1667

1668

1669

1670

1671

1672

1673

1674

1675

1676

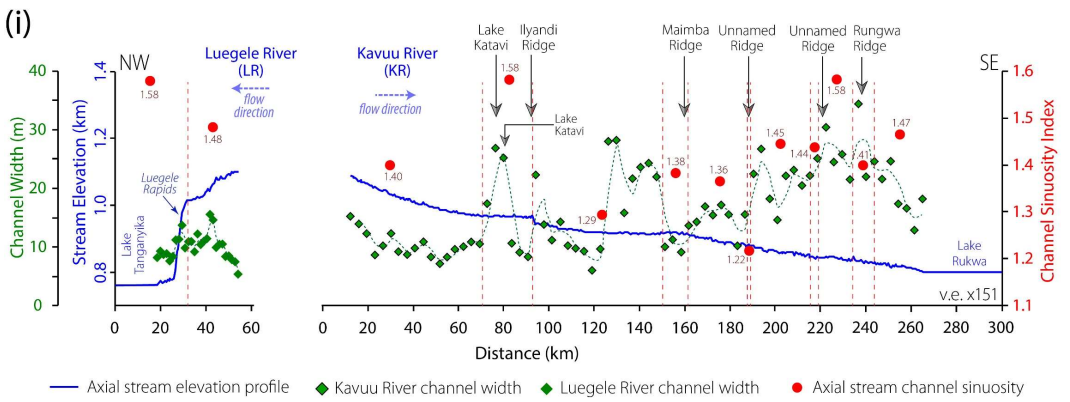
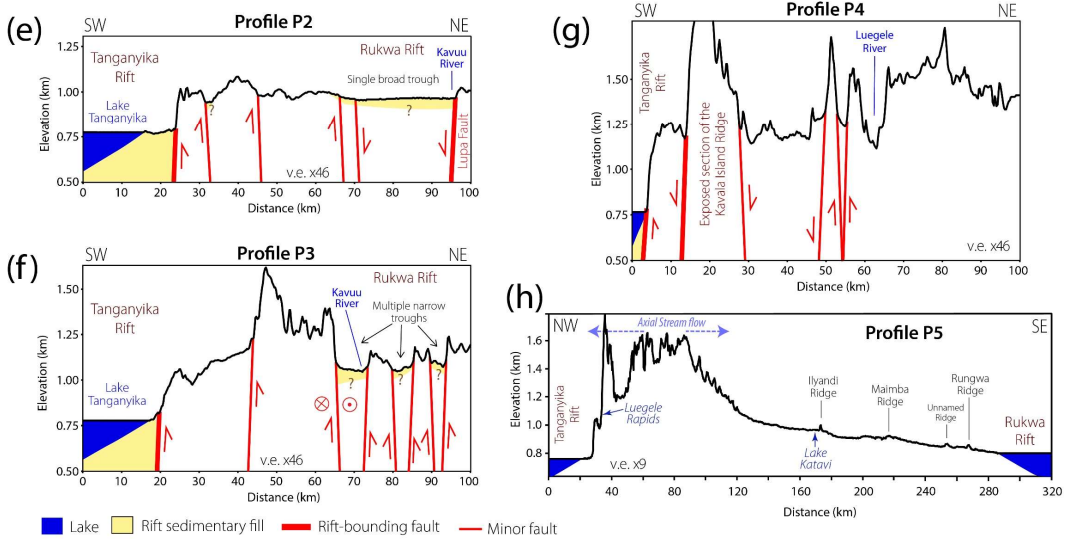
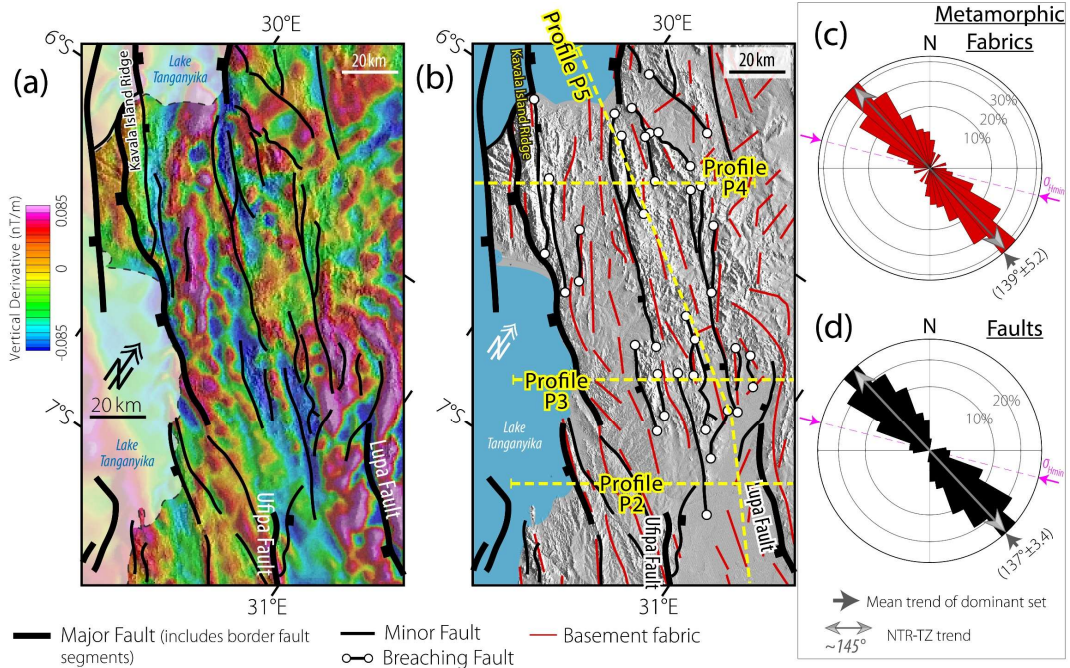
1677

1678

1679

1680

1681
 1682
 1683
 1684
 1685
 1686
 1687
 1688
 1689
 1690
 1691
 1692
 1693
 1694
 1695
 1696
 1697
 1698
 1699
 1700
 1701
 1702
 1703
 1704
 1705



1706 **Figure 6: North Tanganyika–Rukwa Transfer Zone, NTR-TZ (Overlapping Oblique**
1707 **Divergent).** (a.) Filtered aeromagnetic grid of the NTR-TZ, overlaid on satellite digital
1708 elevation model (DEM) hillshade map showing the magnetic fabrics of the basement. (b)
1709 Satellite digital elevation model (DEM) hillshade map overlaid with interpretations of the
1710 interpreted basement fabrics. (c) Frequency-azimuth distribution of the aeromagnetic
1711 basement fabrics in Figure 4b. (d) Frequency-azimuth distribution of the mapped faults
1712 along the transfer zone (Figure 4b). (e – g) Rift-orthogonal topographic profiles showing the
1713 southeast to northwest transition from a single broad rift geometry, through a multi-trough
1714 geometry, and attenuating into a zone of diffused faulting. (h) Transfer zone-parallel
1715 topographic profile showing the salient anomalies that characterize the morphology of the
1716 transfer zone. (i) Longitudinal stream profiles for the main axial streams that intersect the
1717 profile transect (Kavuu and Luegele Rivers).

1718

1719

1720

1721

1722

1723

1724

1725

1726

1727

1728

1729

1730

1731

1732

1733

1734

1735

1736
 1737
 1738
 1739
 1740
 1741
 1742
 1743
 1744
 1745
 1746
 1747
 1748
 1749
 1750
 1751
 1752
 1753
 1754
 1755
 1756
 1757
 1758
 1759
 1760
 1761
 1762
 1763

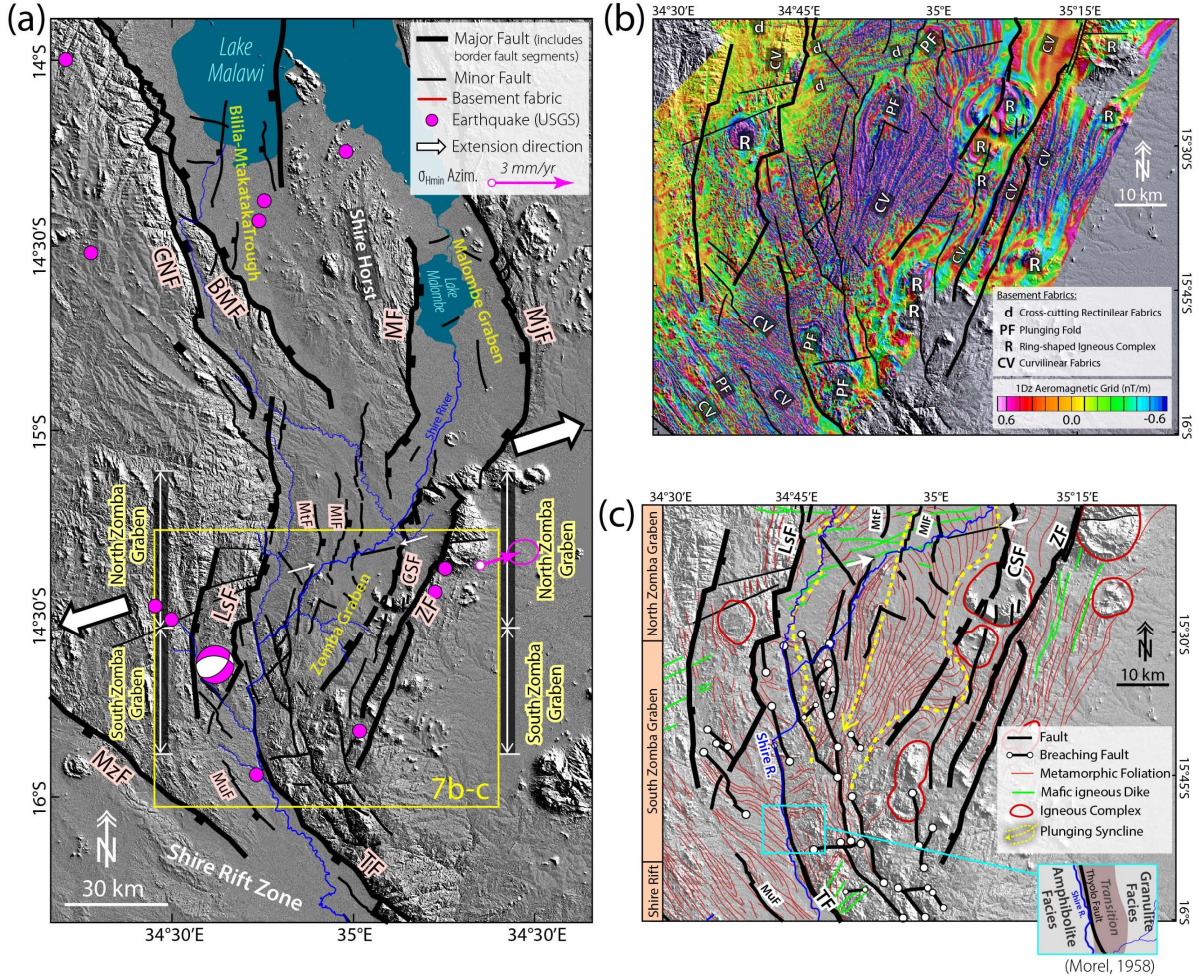


Figure 7: South Malawi–Shire Transfer Zone, SMS-TZ (Overlapping Oblique Divergent). (a.) Satellite Digital Elevation Model (DEM) hillshade map with fault interpretations of the southern Malawi Rift and the northeastern part of the Shire Rift Zone. Fault lineaments are obtained from the satellite DEM and filtered aeromagnetic data interpretation (this study), and previously published satellite DEM and field study (Wedmore et al., 2020). Crustal stretching velocity (green arrow) with 95% uncertainty ellipse is from Stamps et al. (2018).

1764 BMF = Bilila-Mtakataka Fault, CNF = Chirobwe-Ncheu Fault, LsF = Lisungwe Fault, MF =
1765 Malombe Fault, Mlf = Mlungusi Fault, MtF = Mtsimukwe Fault, MuF = Mtumba Fault, MjF =
1766 Mwanjage Fault, MzF = Mwanza Fault, TF = Thyolo Fault, CSF = Chingale Step Fault, ZF =
1767 Zomba Fault. (b) Satellite DEM Hillshade map overlaid with filtered aeromagnetic grid of the
1768 transfer zone. (c) Interpretation of basement fabrics and faults from 7a and 7b. (d - e)
1769 Frequency-azimuth distribution of the rift faults and the inherited pre-rift basement
1770 metamorphic fabrics in the northern (North Zomba) and southern (South Zomba) domains
1771 of the transfer zone.

1772

1773

1774

1775

1776

1777

1778

1779

1780

1781

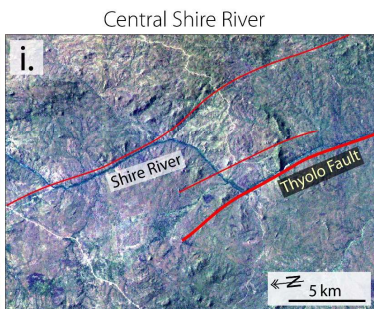
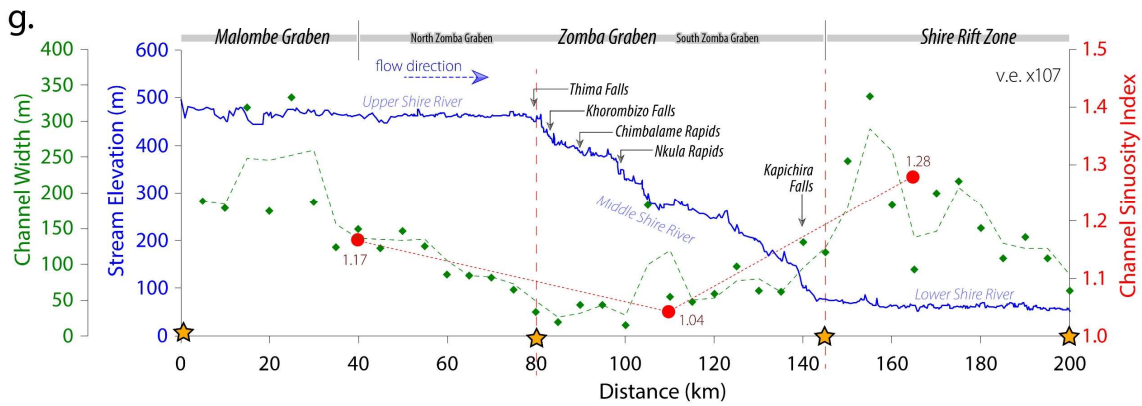
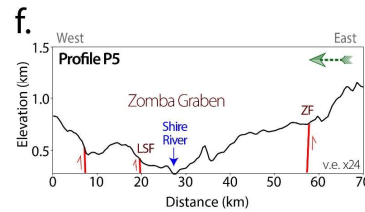
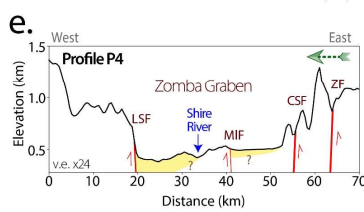
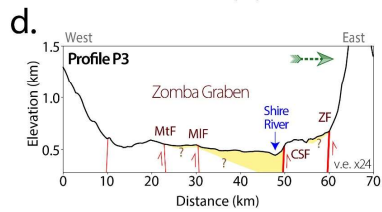
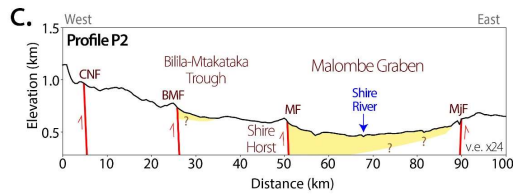
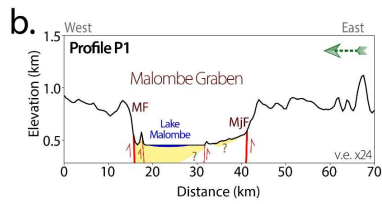
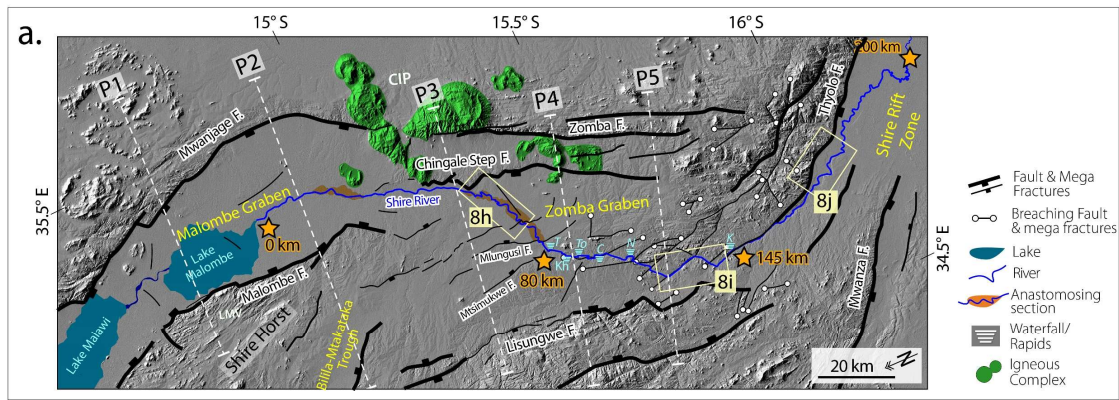
1782

1783

1784

1785

1786



1788 **Figure 8: Axial drainage system of the South Malawi-Shire Transfer Zone, SMS-TZ.** (a.)
1789 Satellite digital elevation model (DEM) hillshade map overlaid with faults and the axial
1790 stream channel (Shire River). C = Chimbaleme (or Machimbeya, or Chilemba) Rapids, CIP =
1791 Chilwa Igneous Province, K = Kapichira Falls, Kh = Khorombizo (or Kholombidzo) Falls, LMV
1792 = Lake Malombe Vents, N = Nkula Rapids, T = Thima Rapids, To = Toni Rapids. (b - f) Rift-
1793 orthogonal topographic profiles showing a north to south variation in rift polarity and the
1794 associated location of the Shire River. (g) Shire River stream profile, channel width, and
1795 sinuosity index estimates. (h - j) Landsat TM false color composites (321RGB) of the (h)
1796 Upper, (i) Middle, and (j) Lower courses of the Shire River. Overall, the unidirectionality of
1797 flow and morphology of the axial stream across the transfer zone cross-over region, linkage
1798 of interacting rift border faults by a cluster of breaching fault/fractures, exposure of pre-rift
1799 basement at the rift-floor (Figure 8i), and an unequilibrated stream profile (Figure 8g)
1800 suggest a recent breaching of the transfer zone.

1801

1802

1803

1804

1805

1806

1807

1808

1809

1810

1811

1812

1813

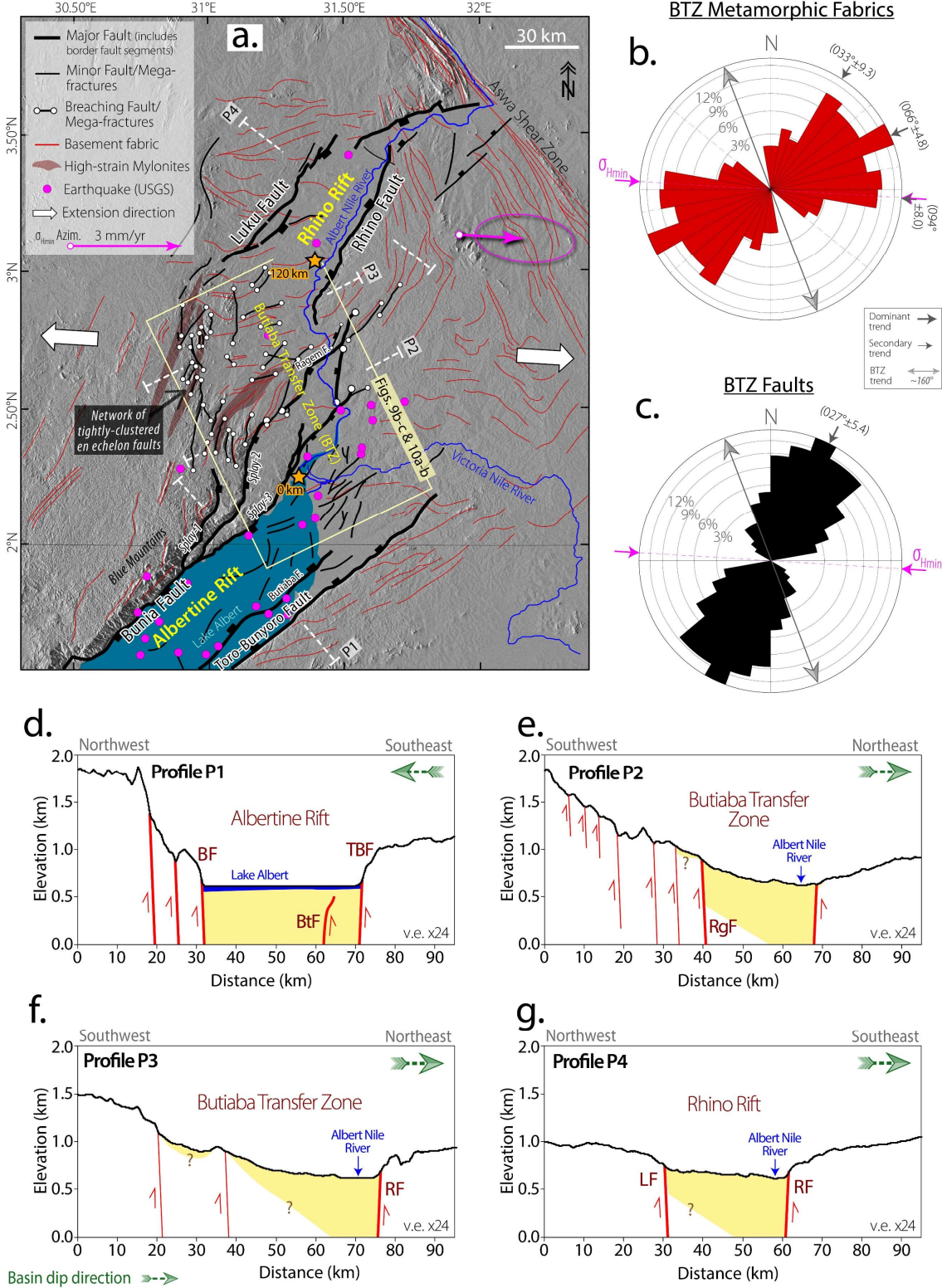
1814

1815

1816

1817

1818
 1819
 1820
 1821
 1822
 1823
 1824
 1825
 1826
 1827
 1828
 1829
 1830
 1831
 1832
 1833
 1834
 1835
 1836
 1837
 1838
 1839
 1840
 1841
 1842



1843 **Figure 9: Albertine–Rhino Rift Transfer Zone, AR-TZ, a.k.a. Butiaba Transfer Zone, BTZ**
1844 **(Underlapping Parallel Divergent).** (a.) Satellite digital elevation model (DEM) hillshade
1845 map overlaid with interpretations of fault and basement fabrics in the Albertine and Rhino
1846 Rifts. Fault lineaments are interpreted from satellite DEM and filtered aeromagnetic data
1847 (this study; Supplementary Figure 3), and from seismic reflection data (Simon et al., 2017).
1848 We also interrogated and included faults segments from other previous studies (GTK
1849 Consortium, 2012; Westerhof et al., 2014; Katumwehe et al., 2015). The locations of highly
1850 strained mylonites are obtained from Westerhof et al. (2014). Crustal stretching velocity
1851 (green arrow) with 95% uncertainty ellipse is from Saria et al. (2014). (b – c) Frequency-
1852 azimuth distribution of the basement fabrics (b) and faults (c) in the transfer zone. (d - g)
1853 Rift-orthogonal topographic profiles showing a southwest to northeast variation in rift
1854 polarity in relation to the location of the axial stream. BF = Bunia Fault, BtF = Butiaba Fault,
1855 LF = Luku Fault; RF = Rhino Fault, RgF = Ragem Fault, TBF = Toro-Bunyoro Fault. Note that
1856 the thickness of the rift sedimentary deposits shown in the topographic profiles are not
1857 drawn to scale.

1858

1859

1860

1861

1862

1863

1864

1865

1866

1867

1868

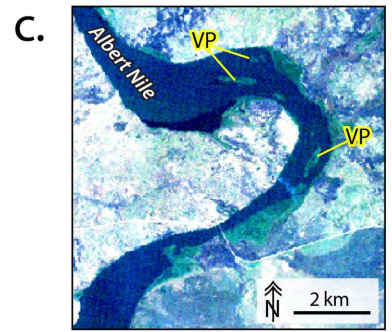
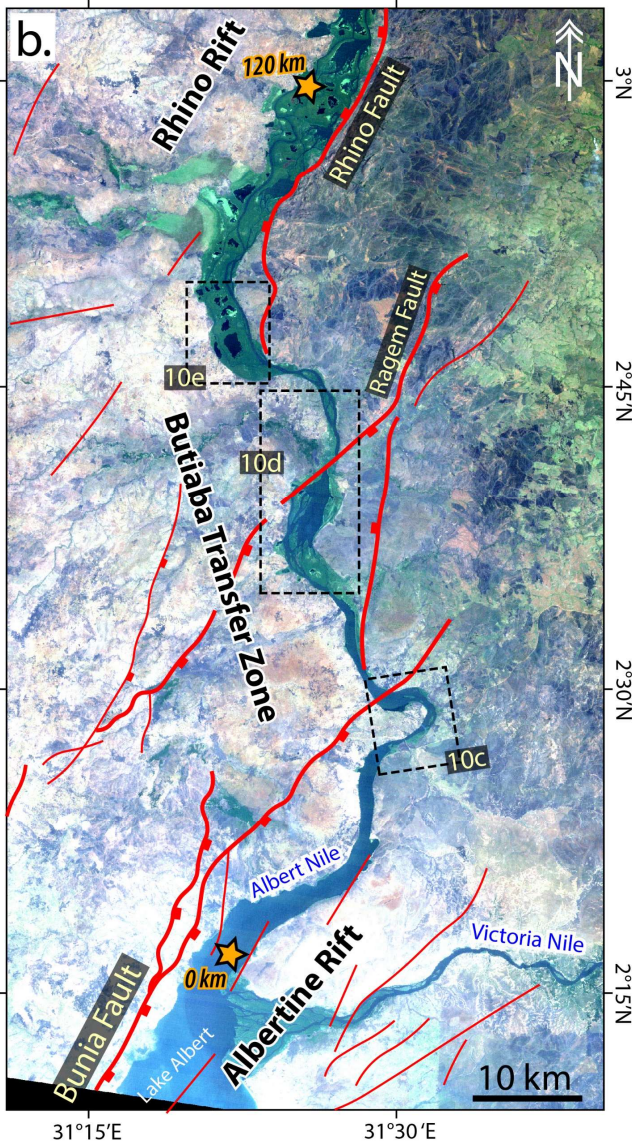
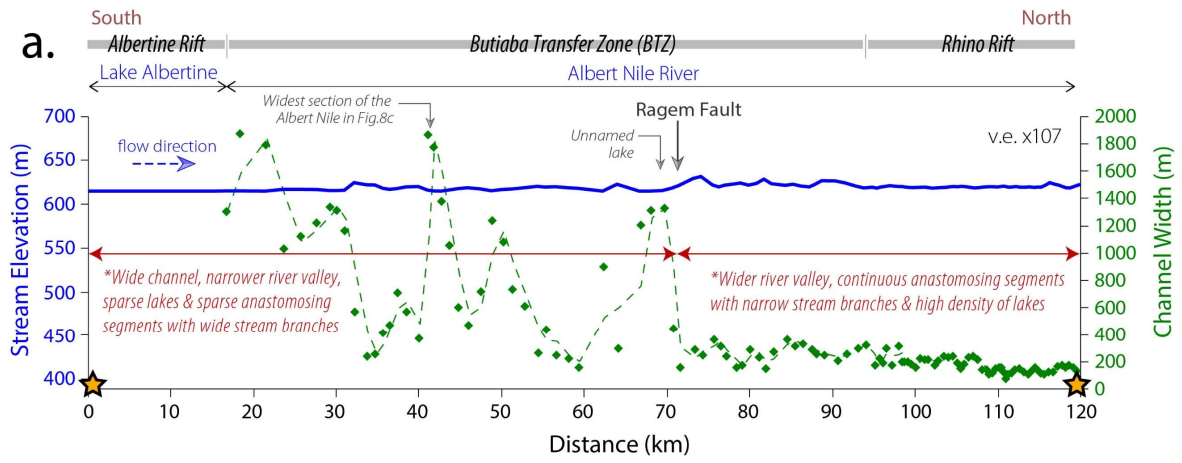
1869

1870

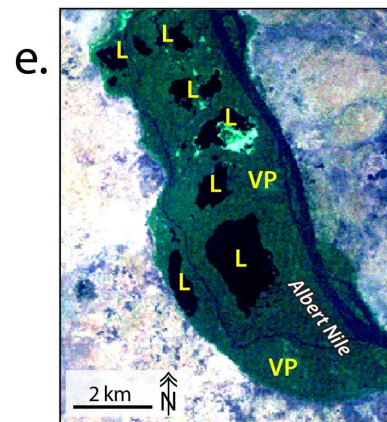
1871

1872

1873



VP = Vegetated point bar L = lake



1875 **Figure 10: Axial drainage system of the Albertine-Rhino Transfer Zone (Butiaba**
1876 **Transfer Zone).** (a.) The Albert Nile River stream profile, and along-channel stream width.
1877 At the anastomosing segments of the river, the profile represents a single branch of the river
1878 with open waters (i.e. not covered by wetland vegetation). (b - e) Landsat TM false color
1879 composite (321RGB) images showing the sinuous and anastomosing morphology of the
1880 Albert Nile River within the transfer zone. L = Lake, VP = vegetated point bar.

1881

1882

1883

1884

1885

1886

1887

1888

1889

1890

1891

1892

1893

1894

1895

1896

1897

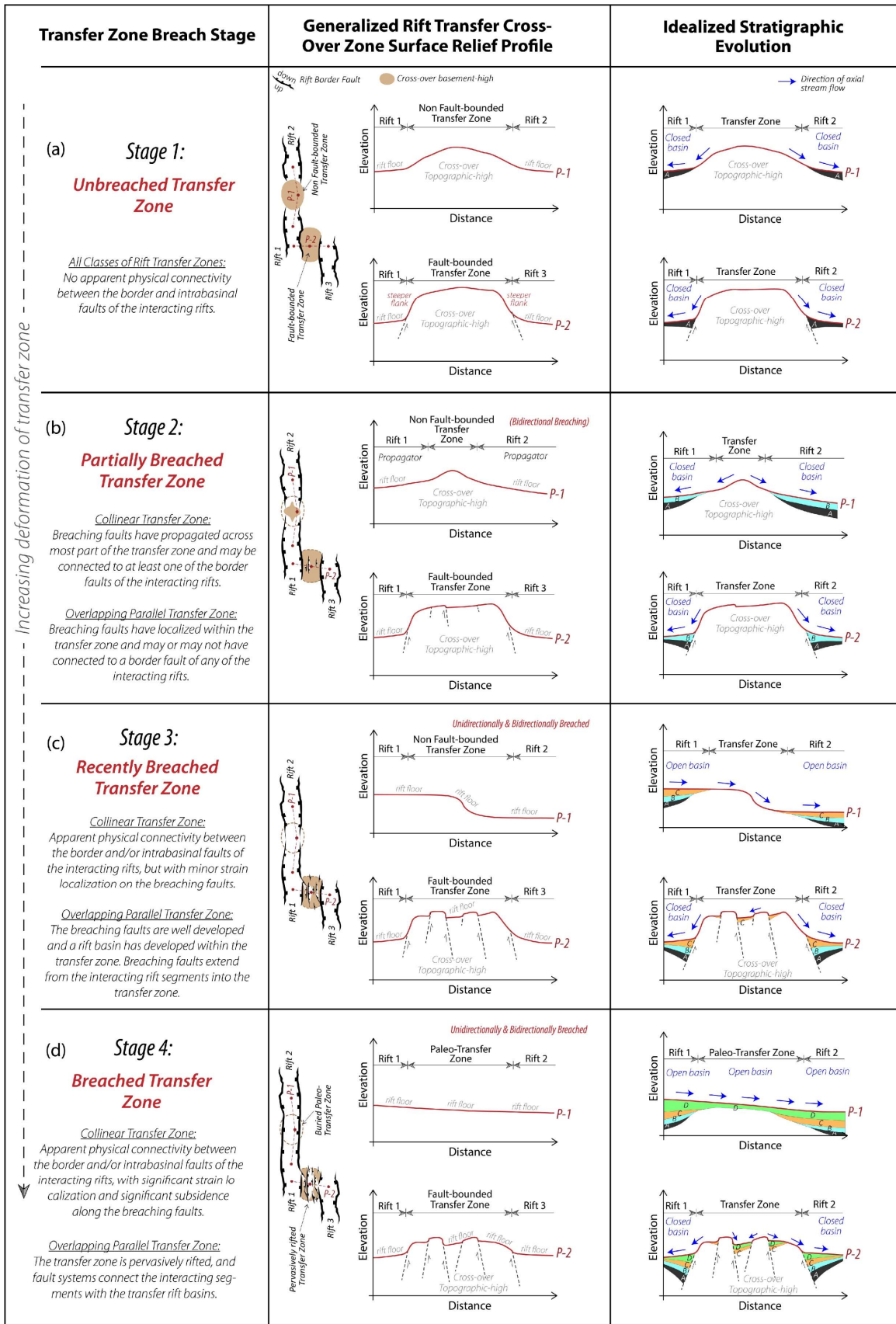
1898

1899

1900

1901

1902
1903
1904
1905
1906
1907
1908
1909
1910
1911
1912
1913
1914
1915
1916
1917
1918
1919
1920
1921
1922
1923
1924
1925
1926
1927



1928 **Figure 11: Models of the stages of evolution of non-magmatic rift transfer zones.** (a – d)
1929 Summary cartoons based on the general observations of structure, long-wavelength
1930 topographic relief, and axial drainage patterns of transfer zones along the western branch of
1931 the East African Rift System (WB-EARS). We present only the tip-to-tip parallel and
1932 overlapping parallel divergent transfer zone geometries as examples to demonstrate our
1933 observations and idealized models. The models assume: 1) humid continental setting, 2)
1934 orthogonal extension, 3) the erodibility of the pre-rift basement is relatively uniform (in the
1935 case of the WB-EARS transfer zones studied), 4) sediment supply in the interacting basins
1936 keeps up with strain rates on faults, and 5) no active dynamic topography in the deforming
1937 transfer zone. The geometry of the breaching faults as presented, are simplified and do
1938 necessarily indicate the kinematics of the breaching structures. Also, note that the
1939 topographic relief geometries of Stages 2 (and possibly Stage 3) are strongly dependent on
1940 the directionality of propagation of rift linkage assuming that basement erodibility is
1941 uniform. These models are based on regions of active early-stage (stretching phase)
1942 continental rifting in which at least one of the interacting rift pairs is active.

1943

1944

1945

1946

1947

1948

1949

1950

1951

1952

1953

1954

1955

1956

1957

1958

1959
1960
1961
1962
1963
1964
1965
1966
1967
1968
1969
1970
1971
1972
1973
1974
1975
1976
1977
1978
1979
1980
1981
1982
1983
1984
1985

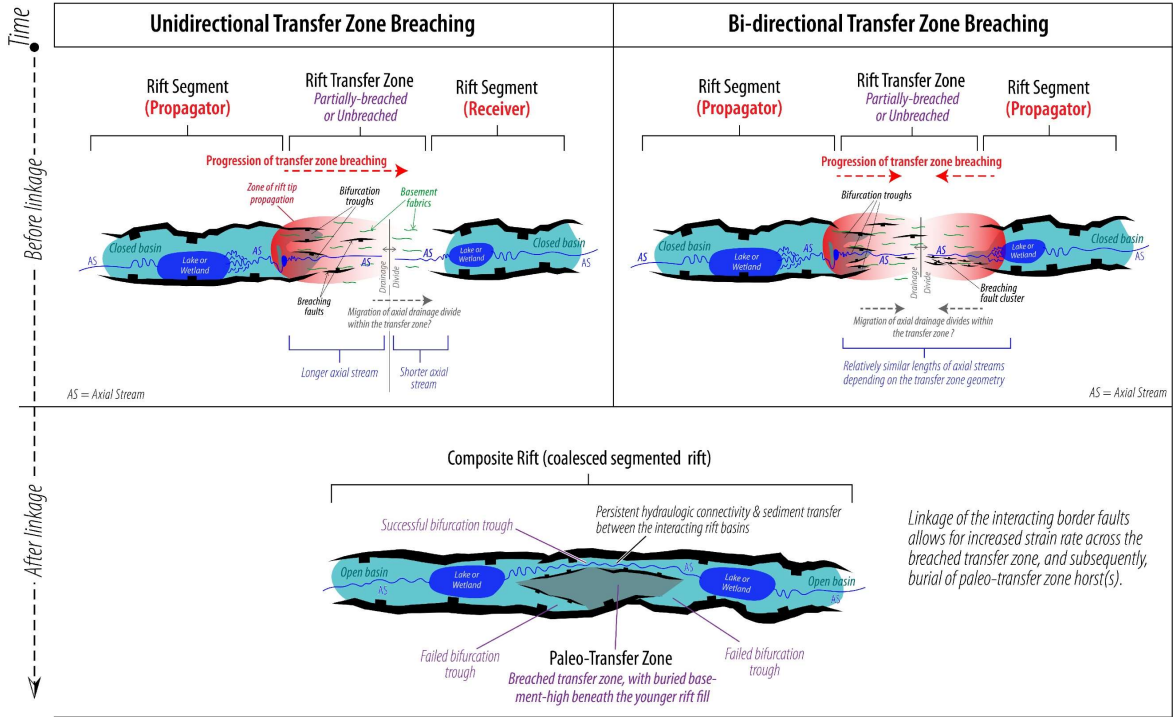
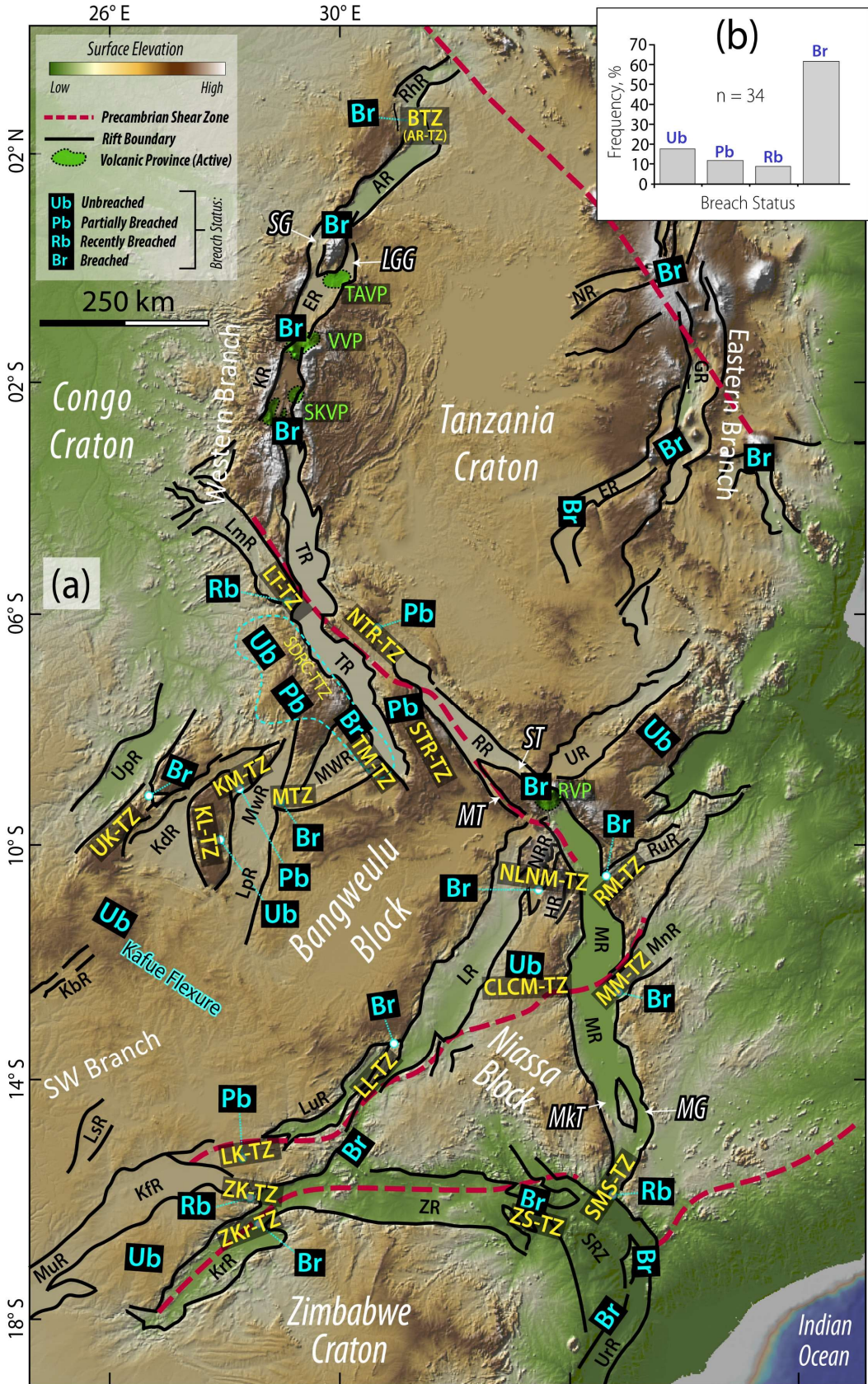


Figure 12: Directional propagation of transfer zone breaching, and rift-tip interactions. Using an active collinear transfer zone as a simple example, these cartoons show directionality of transfer zone breaching and rift tip splay as an example of rift-tip interactions. Other rift tip interactions discussed in the study include border fault rotation and fault cluster networks.

1986
1987
1988
1989
1990
1991
1992
1993
1994
1995
1996
1997
1998
1999
2000
2001
2002
2003
2004
2005
2006
2007
2008
2009
2010
2011



2012 **Figure 13: *Breach-state of rift transfer zones in eastern Africa.*** (a) Map showing the
2013 inferred breach state of the transfer zones along the western, SW, and SE branches of the
2014 East African Rift System, inferred from the general conventions of transfer zone cross-over
2015 structure and physiography proposed in this study. Also note that we characterize all
2016 magmatic transfer zones as “breached” because of the lithospheric-scale deformation
2017 associated with magmatism. SDRC-TTZ = South DRC Rift Zone - Tanganyika Rift Transfer
2018 Zone. See Figure 4a for the explanations of the abbreviated rift and transfer zone labels. Map
2019 Source: Global Multi-Resolution Topography (GMRT) digital elevation model (Ryan et al.,
2020 2009). (b) Histogram of the distribution of the inferred breach states of the rift transfer zones
2021 in Figure 13a.

2022

2023

2024

2025

2026